Magnetic resonance imaging techniques for evaluation of left ventricular function

Pahlm, Ulrika

2018

Document Version:
Publisher's PDF, also known as Version of record

Magnetic resonance imaging techniques for evaluation of left ventricular function

ULRIKA PAHLM
DEPARTMENT OF CLINICAL PHYSIOLOGY | FACULTY OF MEDICINE | LUND UNIVERSITY

"Views of bleeding hearts"
Artist: Chris Wagner

Printed by Media-Tryck, Lund 2018 NORDIC SWAN ECOLABEL 3041 0903

LUND UNIVERSITY

FACULTY OF MEDICINE

Department of Clinical Physiology

Lund University, Faculty of Medicine
Doctoral Dissertation Series 2018:137
ISBN 978-91-7619-705-9
ISSN 1652-8220

Magnetic resonance imaging techniques for evaluation of left ventricular function

Ulrika Pahlm

LUND
UNIVERSITY

DOCTORAL DISSERTATION

Submitted with permission from Faculty of Medicine, Lund University, Sweden.
This thesis will be defended at 09:00 on Thursday, 22 November, 2018 in
Föreläsningssal 3, Blocket, Skåne University Hospital, Lund, Sweden.

Faculty Opponent

Chiara Bucciarelli-Ducci MD, PhD, FESC, FRCP
Consultant Senior Lecturer in Cardiology/Noninvasive Imaging
Bristol Heart Institute, University Hospitals Bristol NHS Foundation Trust

Organization LUND UNIVERSITY	Document name Doctoral dissertation
	Date of issue: 30 October, 2018
Author(s) Ulrika Pahlm	Sponsoring organization Swedish Heart and Lung Association, Lund University

Title and subtitle

Magnetic resonance imaging techniques for evaluation of left ventricular function

Abstract

Myocardial infarction (MI) is the most common cause of death. During an MI, a part of the heart muscle dies due to the lack of oxygen caused by the occlusion of a coronary artery. The function of the heart muscle in the vicinity of the MI is also affected. Exactly how the heart's function is affected during the first days after MI, and how the left ventricle (LV) recovers over time is unclear. Although there are many methods for evaluation of LV function, there is a need to further develop quantitative, reproducible measurements.

Cardiac magnetic resonance imaging (CMR) is used in this thesis in phantom experiments and to study patients, healthy volunteers, and animals. CMR IMAGING is considered to be the most reliable method of measuring cardiac volumes, infarct size and blood flow in the heart.

In study 1, a new method (2 D velocity-coded strain) to evaluate global and regional strain was validated against optical measurements. This method uses 2 D velocity encoded CMR IMAGING images of the heart and was developed by the cardiac MR group at Lund University. A good match was found between measured strain with CMR IMAGING and optical measurements in phantom experiments. The method was tested in 36 healthy volunteers, and reference values for longitudinal strain for the healthy were obtained. When comparing strain results from healthy volunteers to results from 10 patients with recent MI, we found significantly decreased global longitudinal strain in patients compared to the healthy volunteers.

In study 2, 2 D velocity encoded strain and wall thickening (WT), were measured before and after MI in an experimental animal model. The purpose was to investigate how LV function changed acutely after MI and to investigate whether it was possible to differentiate between LV areas with infarction, areas adjacent to and areas remote from the infarction. Analysis showed that it was possible to differentiate between these areas in statistical terms but that the precision was not high enough for use in individual patients.

In studies 3-4, LV function was studied within one week (study 3) and 6 months (study 4) after MI. Study 3 included 177 patients within a week of MI from 2 international research studies and 20 healthy controls. Atrioventricular plane displacement (AVPD) and LV longitudinal strain were measured. Patients had reduced global AVPD and strain compared to the controls. The reduction was found in both infarcted and non-infarcted areas of the LV, i.e. even areas not directly exposed to ischemia were affected. The study also showed that the longitudinal movement of the LV is the main contributor to SV even after MI.

In study 4, a sub-group (n=77) of the patients from study 3 underwent a second CMR imaging study 6 months after STEMI. The study showed that global AVPD improved but remained decreased compared to controls. Patients with left anterior descending (LAD) and right coronary artery (RCA) infarction continued to have decreased AVPD in both infarcted and remote segments of the LV 6 months after STEMI. Wall thickening was decreased in all segments in patients with LAD infarction within a week and 6 months of STEMI. The decrease in WT was more localized around the infarcted area in patients with RCA and left circumflex artery infarction.

Key words: Left ventricular function, Cardiac magnetic resonance, Atrioventricular plane displacement, strain, wall thickening

Classification system and/or index terms (if any)

Supplementary bibliographical information		Language English
ISSN and key title 1652-8220		ISBN 978-91-7619-705-9
Recipient's notes	Number of pages 65	Price
	Security classification	

Signature 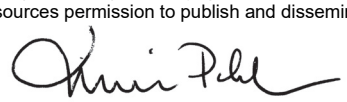 Date 12 October, 2018

Magnetic resonance imaging techniques for evaluation of left ventricular function

Ulrika Pahlm

LUND
UNIVERSITY

Evaluation committee

Associate professor Bengt Johansson
Umeå University, Sweden

Professor Lars Edvinsson
Lund University, Sweden

Associate professor Alexandru Schiopu
Lund University, Sweden

Thesis advisors

Associate Professor Marcus Carlsson, Professor Håkan Arheden,
Associate Professor Einar Heiberg and Associate Professor Henrik Engblom
Lund University, Sweden

Cover: "*Views of bleeding hearts"* (Löjtnantshjärtan)
Artist: Chris Wagner

Department of Clinical Physiology

Lund University, Faculty of Medicine, Doctoral Dissertation Series 2018:137
ISBN 978-91-7619-705-9
ISSN 1652-8220
Printed by Media-Tryck, Lund University, 2018

“Success is not final, failure is not fatal: it is the courage to continue that counts.”

Winston Churchill

Contents

Everything is going to be fine in the end.

If it´s not fine, it´s not the end

Oscar Wilde

List of publications

Paper 1: Longitudinal strain from velocity encoded cardiovascular magnetic resonance: a validation study. Heiberg E, Pahlm-Webb U, Agarwal S, Bergvall E, Fransson H, Steding-Ehrenborg K, Carlsson M, Arheden H. J Cardiovasc Magn Reson. 2013;15:15.

Paper 2: Regional wall function before and after acute myocardial infarction: an experimental study in pigs. Pahlm US, Ubachs JF, Heiberg E, Engblom H, Erlinge D, Götberg M, Arheden H. BMC Cardiovasc Disord. 2014;14:118.

Paper 3: Longitudinal left ventricular function is globally depressed within a week of STEMI. Pahlm U, Seemann F, Engblom H, Gyllenhammar T, Halvorsen S, Steen Hansen H, Erlinge D, Atar D, Heiberg E, Arheden H, Carlsson. Clin Physiol Funct Imaging. 2018;38:1029-37.

Paper 4: Evolution of left ventricular function after ST elevation myocardial infarction. Pahlm U, Ostenfeld E, Seemann F, Engblom H, Erlinge D, Heiberg E, Arheden H, Carlsson M. Manuscript in progress.

Author's contributions

	Study design	Preparation of ethical proposal	Data collection	Data analysis	Statistics	Figures/ Tables	Interpretation of results	Preparation of manuscript	Revision of manuscript	Reply to reviewers
Study 1	2	0	3	3	2	3	3	3	2	2
Study 2	3	0	1	3	3	3	3	3	3	3
Study 3	3	0	0	3	3	3	3	3	3	3
Study 4	3	0	0	3	3	3	3	3	-	-

Not applicable	-
No contribution	0
Limited contribution	1
Moderate contribution	2
Significant contribution	3

Peer-reviewed publications by the author not included in this thesis

1. The standard 11-lead ECG. Neglect of lead aVR in the classical limb lead display. **Pahlm US**, Pahlm O, Wagner GS. J Electrocardiol. 1996;29 Suppl:270-4.
2. Comparison of teaching the basic electrocardiographic concept of frontal plane QRS axis using the classical versus the orderly electrocardiogram limb lead displays. **Pahlm US**, O'Brien JE, Pettersson J, Pahlm O, White T, Maynard C, Wagner GS. Am Heart J. 1997;134(6):1014-8.
3. Comparison of the various electrocardiographic scoring codes for estimating anatomically documented sizes of single and multiple infarcts of the left ventricle. **Pahlm US**, Chaitman BR, Rautaharju PM, Selvester RH, Wagner GS. Am J Cardiol. 1998;81(7):809-15.
4. A new method for using the direction of ST-segment deviation to localize the site of acute coronary occlusion: the 24-view standard electrocardiogram. **Pahlm-Webb U**, Pahlm O, Sadanandan S, Selvester RH, Wagner GS. Am J Med. 2002;113(1):75-8.
5. Maximal increase in sensitivity with minimal loss of specificity for diagnosis of acute coronary occlusion achieved by sequentially adding leads from the 24-lead electrocardiogram to the orderly sequenced 12-lead electrocardiogram. Perron A, Lim T, **Pahlm-Webb U**, Wagner GS, Pahlm O. J Electrocardiol. 2007;40(6):463-9.
6. Use of the 24-lead "standard" electrocardiogram to identify the site of acute coronary occlusion. A review paper. Wagner GS, **Pahlm-Webb U**, Pahlm O. J Electrocardiol. 2008;41(3):238-44.
7. The 24-lead ECG display for enhanced recognition of STEMI-equivalent patterns in the 12-lead ECG. **Pahlm U**, Pahlm O, Wagner GS. J Electrocardiol. 2014;47(4):425-9. Review.
8. Time-resolved tracking of the atrioventricular plane displacement in Cardiovascular Magnetic Resonance (CMR) images. Seemann F, **Pahlm U**, Steding-Ehrenborg K, Ostenfeld E, Erlinge D, Dubois-Rande JL, Jensen SE, Atar D, Arheden H, Carlsson M, Heiberg E. BMC Med Imaging. 2017;17(1):19.
9. Longitudinal shortening remains the principal component of left ventricular pumping in patients with chronic myocardial infarction even when the absolute atrioventricular plane displacement is decreased. Asgeirsson D, Hedström E, Jögi J, **Pahlm U**, Steding-Ehrenborg K, Engblom H, Arheden H, Carlsson M. BMC Cardiovasc Disord. 2017;17(1):208.

If you can dream it, you can do it.

Walt Disney

Summary

Myocardial infarction (MI) is the most common cause of death. During an MI, a part of the heart muscle dies due to the lack of oxygen caused by the occlusion of a coronary artery. The function of the heart muscle in the vicinity of the MI is also affected. Exactly how the heart's function is affected during the first days after MI, and how the left ventricle (LV) recovers over time, are unclear. Although there are many methods for evaluation of LV function, there is a need to further develop quantitative, reproducible measurements.

Cardiac magnetic resonance (CMR) imaging is used in this thesis in phantom experiments and in studies in patients, healthy volunteers, and animals. CMR imaging is considered the most reliable method of measuring cardiac volumes, infarct size, and blood flow in the heart.

In Study 1 a new method of evaluating global and regional strain was validated against optical measurements. This method uses 2D velocity-encoded CMR images of the heart and was developed by the cardiac MR group at Lund University. A good match was found between measured strain with CMR imaging and optical measurements in phantom experiments. The method was then tested in 36 healthy volunteers, and reference values for longitudinal strain for the healthy were obtained. When comparing strain results from healthy volunteers with results from 10 patients with recent MI, we found significantly decreased global longitudinal strain among the patients.

In Study 2, 2D velocity-encoded strain and wall thickening (WT) were measured before and after MI in an experimental animal model. The purpose was to investigate how LV function changed acutely after MI and whether it was possible to differentiate between LV areas with infarction, areas adjacent to infarction, and areas remote from infarction. Analysis showed that it was possible to differentiate between these areas in statistical terms but that the precision was not high enough for use in individual patients.

In Studies 3–4, LV function was studied within 1 week (Study 3) and 6 months (Study 4) after MI. Study 3 included 177 patients within 1 week of STEMI in 2 international research studies and 20 healthy controls. Atrioventricular plane displacement (AVPD) and LV longitudinal strain were measured. Patients had reduced global AVPD and strain compared with the controls. The reduction was found in both infarcted and noninfarcted areas of the LV; i.e., even areas not directly exposed to ischemia were affected. The study also showed that the longitudinal movement of the LV is the main contributor to stroke volume (SV) even after MI.

In Study 4, a subgroup (n=77) of the patients from Study 3 underwent a second CMR imaging study 6 months after MI. The study showed that global AVPD improved but remained decreased compared with controls. Patients with left anterior descending (LAD) or right coronary artery (RCA) infarction continued to have decreased AVPD in both infarcted and remote segments of the LV 6 months after STEMI. Wall thickening was decreased in all segments in patients with LAD infarction within a week and at 6 months after STEMI. The decrease in WT was more localized around the infarcted area in patients with RCA and left circumflex artery (LCx) infarction.

Populärvetenskaplig sammanfattning

Hjärtinfarkt är en av de vanligaste anledningarna till för tidig död. Vid en hjärtinfarkt dör delar av hjärtmuskeln på grund av att den utsätts för mycket kraftig syrebrist när ett kranskärl täpps till. Även hjärtmuskelvävnad i infarktens närhet påverkas. Hjärtats vänsterkammare förser kroppen med syresatt blod. Exakt hur vänsterkammarens funktion påverkas under de första dagarna efter hjärtinfarkt, och hur vänsterkammaren återhämtar sig över tid är inte helt utrett. Trots att det finns många metoder för att utvärdera vänsterkammarens funktion så finns det behov att ytterligare utveckla reproducerbara mått. På så sätt kan förståelsen och diagnostiken av hjärtsjukdomar förbättras.

Magnetisk resonanstomografi, vanligen kallad MR, används i samtliga delarbeten i denna avhandling för undersökning av patienter, friska frivilliga och försöksdjur samt i fantomexperiment. MR anses vara den mest tillförlitliga metoden när det gäller mätning av hjärtats volymer, hjärtinfarktstorlek och blodflöden i hjärtat.

I delstudie 1 utvärderades en ny metod (hastighets-kodad strainmätning), som har potential för klinisk användning, för bestämning av töjning (strain) av vänsterkammarmuskeln. Metoden använder speciella hastighetskodade bilder av hjärtat tagna med magnetkamera och är utvecklad av hjärt-MR gruppen vid Lunds Universitet. När hastighetskodad strain med MR jämfördes med en oberoende, optisk metod i modellförsök påvisades god överensstämmelse. Metoden testades sedan vidare på 36 friska försökspersoner och referensvärden för strain togs fram. Metoden provades också på 10 personer efter hjärtinfarkt och man kom fram till att strain är generellt sänkt hos patienter efter hjärtinfarkt jämfört med friska försökspersoner.

I delstudie 2 mättes strain och väggförtjockning av hjärtats vänsterkammarmuskel före och efter hjärtinfarkt i försöksdjur. Syftet var att undersöka hur vänsterkammarens funktion förändrades akut efter hjärtinfarkt och att undersöka om det var möjligt att skilja på områden med infarkt, områden nära och områden långt från infarkten med hjälp av strain och väggförtjockning. Resultatet blev att dessa områden uppvisade klara skillnader i statistiskt hänseende men att precisionen inte var tillräckligt hög för att kunna användas på patienter.

I delstudie 3 undersöktes vänsterkammarens funktion hos 177 patienter från 2 internationella forskningsstudier en vecka efter hjärtinfarkt samt hos 20 friska frivilliga försökspersoner. Förkortning av vänsterkammaren under hjärtcykeln, strain i vänsterkammarväggen samt väggförtjockning undersöktes i olika delar av vänsterkammaren. Resultaten visade sänkt vänsterkammarfunktion avseende både förkortning, strain och väggförtjockning hos patienter efter hjärtinfarkt jämfört med

friska försökspersoner. Den sänkta funktionen påvisades både i områden med infarkt och områden utan infarkt, dvs. även i delar av hjärtmuskeln som inte varit utsatta för syrebrist. Den sänkta funktionen stod i proportion till infarktstorleken.

I delstudie 4 undersöktes 77 patienter från delstudie 3 som genomgått ytterligare en MR-undersökning 6 månader efter hjärtinfarkten. Studien visar att det skedde en viss förbättring av vänsterkammarfunktionen mellan undersökningstillfällena men att funktionen var fortsatt sänkt, både i områden med och utan infarkt.

Abbreviations

ANOVA	analysis of variance
AV	atrioventricular
AHA	American Heart Association
AVPD	atrioventricular plane displacement
CAD	coronary artery disease
CMR	cardiovascular magnetic resonance
CO	cardiac output
ECG	electrocardiogram, electrocardiography
ED	end-diastole
EDV	end-diastolic volume
EF	ejection fraction
ES	end-systole
ESV	end-systolic volume
DENSE	displacement encoding with simulated echoes
FFE	fast-gradient field echo
HF	heart failure
HR	heart rate
ICC	intra class correlation
IS	infarct size
LAD	left anterior descending artery
LCx	left circumflex coronary artery
LGE	late gadolinium enhancement
LV	left ventricle
LVM	left ventricular mass
MAPSE	mitral annular plane systolic excursion
MI	myocardial infarction
MPS	myocardial perfusion study
MR	magnetic resonance
MRI	magnetic resonance imaging
MSI	myocardial salvage index
PCI	percutaneous coronary intervention
RCA	right coronary artery
RF	radio frequency
ROC	receiver operating characteristic
ROI	region of interest
RV	right ventricle
SENC	strain encoding
SPECT	single photon emission computed tomography

SSFP	solid-state free precession
STEMI	ST-segment-elevation myocardial infarction
SV	stroke volume
TAPSE	tricuspid annular plane displacement
TFE	turbo-gradient field echo
WT	wall thickening

"Feeling gratitude and not expressing it is like wrapping a gift and not giving it."

William Arthur Ward

Acknowledgements

I am very thankful to each person who helped me throughout this quite long process. “It takes a village” to write a research paper, not to mention a thesis. The road has been long and winding and I am happy to finally have arrived.

I would especially like to express my gratitude to the following:

My main supervisor **Marcus Carlsson**, who is able to find the perfect balance between coaching and supervising.

My co-supervisor **Håkan Arheden**, who made this thesis possible by taking me on as a PhD student even though I was living in the United States at the time. My co-supervisor **Einar Heiberg**, for fun phantom experiments and great conversations, and co-supervisor **Henrik Engblom**, for friendly support.

My first research mentor **Galen Wagner,** who sadly passed away 2 years ago. I am very grateful for all the amazing opportunities he gave me and for his friendship.

All members of the Cardiac MR group. In this group, the whole is much greater than the sum of the parts. Members support and challenge each other, and I feel privileged to be a member. I especially want to thank **Mikael Kanski** and **David Nordlund** for allowing me to take part in experiments, **Ellen Ostenfeldt** for always cheering me on, **Felicia Seemann** for showing interest in AV-plane movement, **Sebastian Bidhult** for explaining MRI and help with computer stuff, and **Tom Gyllenhammar** for interesting conversations about research and life.

Thank you, **Kerstin Brauer**, for all the help you have given to me throughout the years, and **Ann-Helen Arvidsson** and **Christel Carlander** for all sorts of help with CMR imaging data**.**

My mother, **Elisabet Carneskog-Pahlm**, and father, **Olle Pahlm**, for your love and ongoing help and support in all imaginable ways. My brother **Fredrik Pahlm** and my sister **Sofia von der Goltz and their families** for unconditional love and constant backing in everything I do. I am fortunate to be part of this family.

Lastly, I want to thank my sons, **Alexander Webb** and **Jonathan Webb**. I am very lucky to be your mom. Thank you for cheering me on in my pursuit of the “black hat.” Never forget that I love you to the moon and back.

The studies were supported by the Swedish Heart and Lung Foundation and Lund University.

“The beginning is the most important part of the work.”

Plato

1. Introduction

Heart disease is very common and is linked to high morbidity and mortality (1)(2)(3). Coronary artery disease (CAD) is caused by atherosclerosis in the coronary arteries, which can gradually or suddenly obstruct and stop blood flow to the heart muscle. Although there has been a reduction in CAD mortality in Europe over the past 2 decades, the incidence is still high (4).

Myocardial infarction (MI) is one manifestation of CAD. When a coronary artery is occluded by a thrombus, most often an ST-segment-elevation MI (STEMI) occurs. STEMI is distinguished from other forms of MI through its appearance on an electrocardiogram (ECG). The incidence of STEMI was 58/100,000 per year in Sweden in 2015 (5). In-hospital mortality of STEMI varies between 4% and 12% in European countries (6). For a STEMI patient, it is important to restore normal blood flow in the coronary artery as soon as possible. This is preferably done by percutaneous coronary intervention (PCI) (7) within 2–3 hours of symptom onset.

MI can sometimes lead to heart failure (HF). Approximately 1%–2% of the adult population in developed countries suffer from HF, and in people older than 70, approximately 10% are affected (8)(9)(10)(11). The 12-month all-cause mortality rate for patients hospitalized for acute HF in Europe is about 24%, and it is 6% for patients with chronic HF (12).

Cardiac pathophysiology is quite complex. Several aspects of cardiac function must therefore be assessed in a patient with (suspected) heart disease. Disease processes can affect heart function regionally or globally. Systolic and diastolic function measurements reflect the contraction and relaxation phases of the heart, respectively. Left- and right-sided, and atrial and ventricular function refer to the performance of specific anatomical cardiac structures. New and improved methods are needed to accurately quantify cardiac function in order to distinguish normal from abnormal, to evaluate the severity of disease, to monitor changes, to evaluate the effect of therapy, and to predict prognosis.

Cardiac magnetic resonance imaging is the gold-standard method for measuring cardiac volumes, mass (13), function (14)(15)(16), and MI size (17). The purpose of this thesis is to explore new techniques for quantifying global and regional left ventricular (LV) systolic function by means of CMR imaging in healthy people and in patients after STEMI.

Study 1 introduces and validates a new method for measuring myocardial strain and presents normal values. In Study 2, this method and wall thickening (WT) measurements are used to differentiate between normal and ischemic myocardium. In Study 3, global and regional longitudinal LV function is assessed by LV strain

and atrioventricular plane displacement (AVPD) in patients within a week of STEMI (sub-acute phase) and is compared to controls. A sub-group of the patients in Study 3 were followed up after 6 months (chronic phase). In Study 4 the evolution of LV function between the sub-acute phase and the chronic phase after STEMI is evaluated using AVPD and WT.

Cardiac anatomy

The heart is positioned in the mediastinum, shielded by the ribcage. It is enclosed in the pericardium, a multilayered sack around the heart and vessels entering and leaving it. The pericardium contains a small amount of fluid that reduces friction as the heart moves inside it. The heart contains 4 cavities—2 atria and 2 ventricles. The atria and ventricles are separated from each other by the atrioventricular (AV) plane, a fibrous structure that contains the heart valves. The right and left sides of the heart are separated by the septum, and each side contains 1 atrium and 1 ventricle.

The heart muscle, or myocardium, consists of myocytes that can contract. The epicardium is the outermost layer of the wall and contains the coronary arteries. The endocardium is the thin layer of cells lining the cavities. Myocardial fiber orientation varies continuously from epicardium to endocardium (longitudinal to circumferential to longitudinal) (18). The left ventricular myocardium is thicker than the right, since the resistance of the systemic circulation is 4–5 times higher than that of the pulmonary circulation.

Three coronary arteries supply the heart with blood. Although there is variability in LV coronary artery distribution, as a rule, the left anterior descending (LAD) coronary artery supplies blood to the anterior, anteroseptal, and anterolateral LV walls as well as the apex (19); the right coronary artery (RCA) supplies the inferoseptal, inferior, and inferolateral walls; and the left circumflex (LCx) coronary artery supplies the inferolateral and anterolateral walls (19).

Cardiac physiology

The right atrium receives oxygen-depleted blood from the body through the inferior and superior venae cavae, and the blood then passes through the tricuspid valve into the right ventricle (RV). The RV pumps the blood through the pulmonary valve and the pulmonic trunk into the lungs, where the blood is oxygenated. The blood returns to the heart through the 4 pulmonary veins into the left atrium. The blood flows through the mitral valve into the LV and is ejected through the aortic valve to the systemic circulation (Figure 1.1).

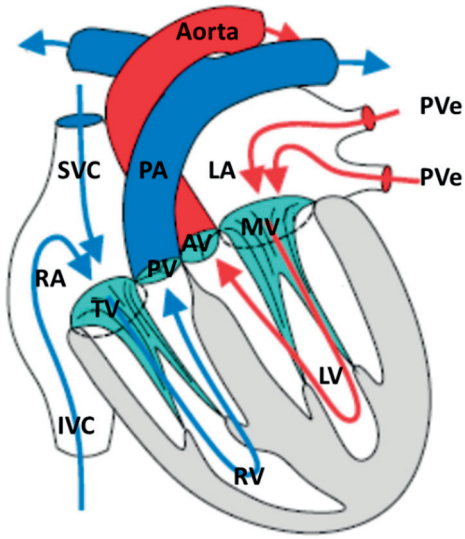

Figure 1.1. Oxygen-depleted blood (blue) returns from the upper and lower parts of the body through the superior vena cava (SVC) and the inferior vena cava (IVC) to the right atrium (RA). The blood passes through the tricuspid valve (TV) to the right ventricle (RV) and is pumped to the lungs through the pulmonary valve (PV) and the pulmonary artery (PA). Oxygenated blood (red) returns to the heart from the lungs via the pulmonary veins (PVe), entering the left atrium (LA). It passes through the mitral valve (MV) to the left ventricle (LV), from which it is ejected through the aortic valve (AV) to the aorta. Adapted from Jonson B, Wollmer P, editors. Klinisk Fysiologi. Stockholm: Liber; 2011.

Left ventricular contraction is rather complex due to the myocardial fiber orientation (18)(20). The subepicardial fibers are oriented in a longitudinal direction in a slightly left-handed helix. The sub-endocardial fibers are also oriented in a longitudinal direction in a right-handed helix, and the midwall fibers are mostly circumferentially oriented (18)(20)(21). Myocardial contraction leads to longitudinal and circumferential shortening, radial thickening, and torsion (22) of the LV. In early systole, before longitudinal shortening, the LV base rotates counterclockwise. Shortly thereafter, longitudinal shortening, clockwise rotation of the base, and counterclockwise rotation of the apex occur (23). As the LV shortens longitudinally, circumferential and longitudinal shortening cause the myocardium to thicken in the endocardial radial direction, reducing the inner diameter of the LV (24). There is only small change in the epicardial, outer diameter of the LV, and the total heart volume varies only 5%–11 % over the heart cycle (25).

In systole, the myocardium contracts, and the papillary muscles pull the AV plane towards the apex. The apex remains quite stationary (26). The descent of the AV plane increases intraventricular pressure, and the mitral and tricuspid valves close. Shortly thereafter, the aortic and pulmonary valves open due to the increased

intraventricular pressure, and blood is ejected into the pulmonary and systemic circulation. Simultaneously, blood is pulled into the atria from the pulmonary and systemic circulation because of the suction created by the AV-plane movement. During diastole, the myocardium relaxes, and the AV plane moves away from the apex. This movement creates negative intraventricular pressure, causing the mitral and tricuspid valves to open and blood flows from the atria into the ventricles. The aortic and pulmonary valves close as soon as blood flow in their respective arteries is reversed.

Cardiac output (CO) is the volume of blood delivered to the body each minute. It is the product of the stroke volume (SV) and the heart rate (HR). SV is the effect of the reduction in LV volume during systole caused by longitudinal and radial shortening (27).

Longitudinal contribution to SV is approximately 60% in healthy adults (28)(29), athletes (28)(30), patients with dilated cardiomyopathy (28), and patients after MI (31). Wall thickening ("radial contribution") contributes the remaining 40% (32), which can be further divided into septal and non-septal-radial (also called lateral) contributions. Septal contraction has been found to contribute 8%–10% of the LV SV in healthy adults (33) (29), and lateral contraction 26%–36% (29).

The electrical conduction system

Myocardial cells (myocytes) have special properties that make them depolarize (and contract) and repolarize (and relax) spontaneously at regular intervals. The electrical impulse that generates the heartbeat normally originates in the sinus node, located in the upper lateral part of the right atrium, and then spreads through the atria. The impulse travels through the AV node and reaches the ventricular myocardium via the ventricular conduction system. It consists of the bundle of His, the left and right bundle branches, and the Purkinje fibers (Figure 1.2). This system enables synchronized ventricular contraction.

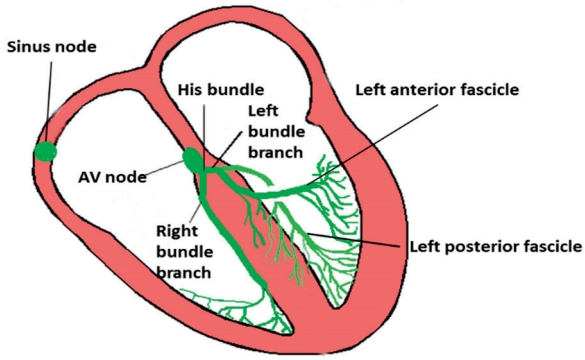

Figure 1.2. The electrical conduction system of the heart. A heartbeat is initiated by spontaneous depolarization of cells in the sinus node, located in the upper right atrium. Depolarization spreads through the atria, causing atrial contraction. It is delayed in the AV node and then progresses to the bundle of His, which divides into the right and left bundle branches. Adapted from Jonson B, Wollmer P, editors. Klinisk Fysiologi. Stockholm: Liber; 2011.

Electrocardiogram

An electrocardiogram (ECG) records the heart's electrical activity on the body surface. It can be displayed on screen or on paper. Figure 1.3 shows the electrode placement on the body and a normal 12-lead ECG.

Standardized terminology is used for waves and intervals in the ECG (Figure 1.4). Atrial contraction is reflected by the P wave, and ventricular contraction by the QRS complex. The ST segment and the T wave reflect ventricular repolarization. The ST segment in the normal ECG is typically at the same level (voltage) as the PR segment. However, it is most often elevated during MI due to an abnormal voltage gradient (injury current) between normal and ischemic myocardium.

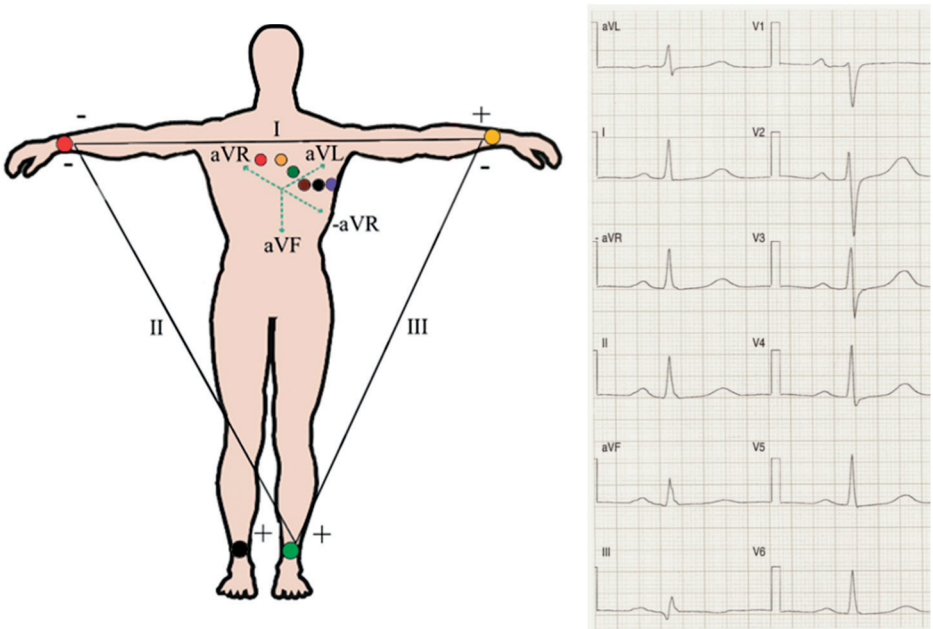

Figure 1.3. Left: When recording a 12-lead ECG, electrodes are placed on 6 anatomically defined positions on the torso and on the extremities. Right: The ECG machine prints the ECG or displays it on screen. ECG leads aVL, I, -aVR, II, aVF, and III display electrical phenomena in the frontal place from the upper left to the lower right part of the body, and leads V1, V2, V3, V4, V5, and V6 display them in the transverse plane from right anterior to left lateral positions. The ECG leads thus "view" the heart from various vantage points.

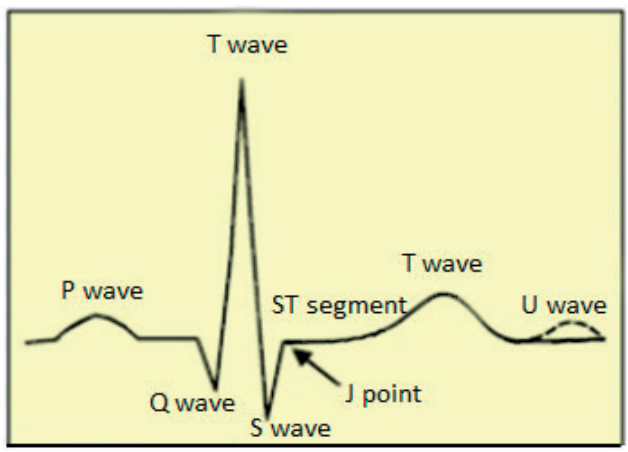

Figure 1.4. Nomenclature for waves and segments in the electrocardiogram.

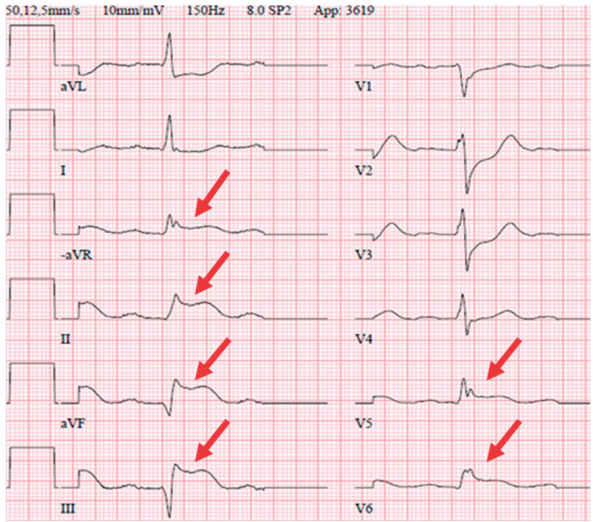

Figure 1.5. 12-lead ECG exhibiting a STEMI pattern due to acute occlusion of a coronary artery. ST-segment elevation is present in several ECG leads (arrows)

Myocardial infarction

Myocardial infarction is caused by occlusion of a coronary artery resulting in ischemia and ultimately death of the myocytes downstream from the occlusion, unless blood flow is restored. Typical symptoms include chest discomfort or pain, and shortness of breath, often accompanied by nausea or vomiting (34). Sometimes the presenting symptom of MI is sudden death due to lethal arrhythmia.

ST-segment-elevation MI (STEMI) (Figure 1.5) exhibits significant elevation of the ST-segment on an ECG, whereas non-ST-segment-elevation MI (NSTEMI) (35) does not. Infarction patterns are often dynamic, i.e., an NSTEMI pattern may evolve to a STEMI pattern and vice versa. Current ECG criteria for STEMI (Table 1.1) are presence of significant ST-segment elevation in at least 2 contiguous ECG leads without the presence of left bundle branch block or left ventricular hypertrophy (2) (36). ST-segment depression in leads V1–V3 can also indicate acute coronary occlusion, and this has been termed a "STEMI-equivalent pattern," especially if the terminal T-wave is positive (36).

Table 1.1. STEMI criteria from the 4th universal definition of myocardial infarction (36)

	Leads V2–V3	Other leads
Men <40 years	≥2.5 mm	≥1 mm
Men >40 years	≥2.0 mm	≥1 mm
Women	≥1.5 mm	≥1 mm

Heart failure after myocardial infarction

Heart failure (HF) is the result of an inability of the heart to deliver enough blood to meet the metabolic demands of the body (37). Insufficient delivery of oxygenated blood leads to several adaptive responses, including cardiac remodeling, activation of the renin-angiotensin-aldosterone system, increased sympathetic activity, and endothelin activation. Typical symptoms and signs include dyspnea on exertion, ankle swelling, fatigue, jugular venous distension, and crackles on lung auscultation. The current definition of HF is restricted to stages in which clinical symptoms are present (9). The presence and degree of clinical HF does not necessarily correlate with global measures of LV function, such as ejection fraction (EF) (9). HF patients may have reduced (38) or normal EF (39)(9), and asymptomatic patients may have altered LV function (40). Patients who survive MI are at risk of developing HF (41), but it remains difficult to identify those who will do so (2). HF after MI is also quite common in patients who have undergone PCI (42).

The structural and geometric changes that may occur after MI (43) are called LV remodeling. This occurs particularly if the MI is large and transmural (44). Adverse LV remodeling implies a clinically significant increase in end-diastolic volume (EDV) (15%–20% or more). It occurs in about one third of patients after MI (45), can lead to HF, and is linked to poor prognosis (46). It is important to identify patients with high likelihood of adverse LV remodeling after STEMI, to prescribe more aggressive management (47) and plan for closer follow-up.

Decreased regional LV function is seen acutely in both ischemic and surrounding areas. The resulting MI decreases function due to edema and replacement of myocytes with fibrosis. LV function will eventually recover in regions that were ischemic but where the myocardium was not infarcted. This recovery takes time. The depressed function after ischemia is called postischemic stunning (48). In contrast, hibernation is defined as decreased LV function caused by decreased perfusion without infarction in patients with chronic CAD. There have also been reports of reduced function in remote areas of the LV after LAD MI (49), but this has not been widely recognized.

American Heart Association 17-segment model

The LV can be divided into a number of segments. The American Heart Association (AHA) recommends a division into 17 segments for regional analysis of LV function or myocardial perfusion (50), and the AHA model was used in this thesis (Figure 1.6).

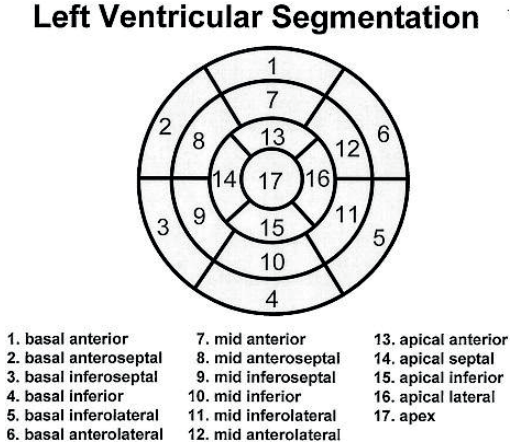

Figure 1.6. American Heart Association 17-segment model. Reproduced from Cerqueira MD et al. J Nucl Cardiol. 2002;9:240-5. © SNM.

Magnetic resonance imaging (MRI)

MRI is a complex imaging technique that uses nuclear magnetic resonance. Since hydrogen is abundant in the body, it is the most commonly used nucleus in medical MRI.

In the magnetic field in the MRI machine, protons aligning either towards or against the magnetic field have a magnetic moment. This magnetic moment has a so-called resonance frequency, the Larmor frequency ($\boldsymbol{\omega_0}$), which is proportional to the field strength of the external magnetic field (B_0) and is calculated by the following formula:

$$\omega_0 = \gamma B_0$$

where ω_0 is the precession rate, γ is the gyromagnetic ratio (constant for each element), and B_0 is the magnetic field strength, measured in Tesla (T).

The precession rate for a hydrogen proton is 42.6 MHz in a magnetic field strength of 1 T.

For imaging, a radiofrequency (RF) pulse (with the same frequency as the Larmor frequency) is transmitted to the protons. This results in a magnetic resonance signal from the protons, which has frequency ω_0. The magnetic resonance signal induces an electrical current that can be picked up by a receiver antenna. When the RF pulse is turned off, protons return to their original state in the external magnetic field.

To determine the origin of the MRI signal within the body, magnetic fields with different field strengths are applied at each point of the patient's cross-section.

Cardiovascular magnetic resonance

It is challenging to perform CMR imaging due to cardiac and respiratory motion. The timing of image acquisition is tied to the R-wave on a simultaneously monitored ECG (51); this is called ECG gating and can be performed prospectively or retrospectively. In prospective ECG gating, the image-acquisition process is started each time an R wave is detected. A consequence of this approach is that the last part of the cardiac cycle is omitted while the system waits for the next trigger pulse. In retrospective gating, the images are continuously sampled and thereafter sorted according to their timing relative to the ECG. For short image acquisition (<20 seconds), patients hold their breath to minimize artifacts due to respiratory motion. When longer acquisitions are needed, respiratory gating is used (52).

Radionuclide imaging of the heart

In single-photon emission computed tomography (SPECT), ^{99m}Tc-labeled tetrofosmin is injected into a peripheral vein. Tetrofosmin is extracted from the bloodstream by the myocytes in proportion to regional blood flow, and it attaches to the mitochondria.

Images of the distribution of ^{99m}Tc in the myocardium are made by a gamma camera. For the animal studies in this thesis, a dual-head camera (ADAC Vertex, Milpitas, CA, USA) was used. Images were collected in 32 projections (40-s collection time per projection) into a 64 × 64 matrix, yielding a digital resolution of 5 × 5 × 5 mm. Short- and long-axis images of the LV were obtained. Automatic segmentation of the LV was performed (53), and the isotope uptake was displayed as a bull's-eye image (Figure 1.7, left circle) (54). Myocardium with less than 50% of the maximum counts was considered ischemic.

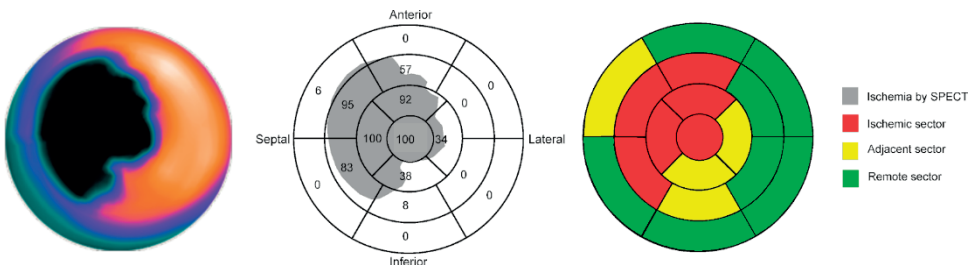

Figure 1.7. The left circle shows the SPECT image. The middle circle shows the relative degree of ischemia according to SPECT presented in the AHA 17-segment model. The right circle shows the classification of the segments according to the degree of ischemia.

Measures of left ventricular function

Ejection fraction (EF) is the most common measure of LV function. It is the percentage of blood ejected from the LV with each heartbeat, thus reflecting changes of cardiac volumes during a heart cycle. It is easily obtained bedside with echocardiography and can be measured by CMR imaging and other imaging modalities. Ejection fraction is used in clinical decision-making and therapy guidance, as well as for diagnosing HF. However, nearly half of the patients with HF symptoms have preserved EF (9). Predictive outcome scores for patients with HF often use EF as one of several predictors (55)(56)(57). EF provides prognostic information after MI (9) but has relatively low sensitivity to subtle decreases in systolic LV function, and it does not provide information on regional function.

Atrioventricular plane displacement is used to quantify longitudinal LV function. To determine AVPD, the position of the AV plane is identified in 6 locations (anterior, anteroseptal, inferoseptal, inferior, inferolateral, and anterolateral) of the LV in end-diastole (ED) and end-systole (ES) using echocardiography or CMR imaging (Figure 1.8). Atrioventricular plane displacement was determined by subtracting the perpendicular AV position in ES from that in ED for each location (58). AVPD can be reported for each location or as global AVPD, i.e., the mean movement of all the AV-plane locations. Global AVPD is in the range of 13–19 mm in healthy individuals (59)(58)(60). Mitral annular plane systolic excursion (MAPSE) and tricuspid annular plane displacement (TAPSE) are other ways to measure AV-plane movement and can be obtained by CMR imaging or echocardiography. Reduced MAPSE is a marker of LV systolic dysfunction in patients with hypertension, and it can diagnose HF in patients with preserved EF (61).

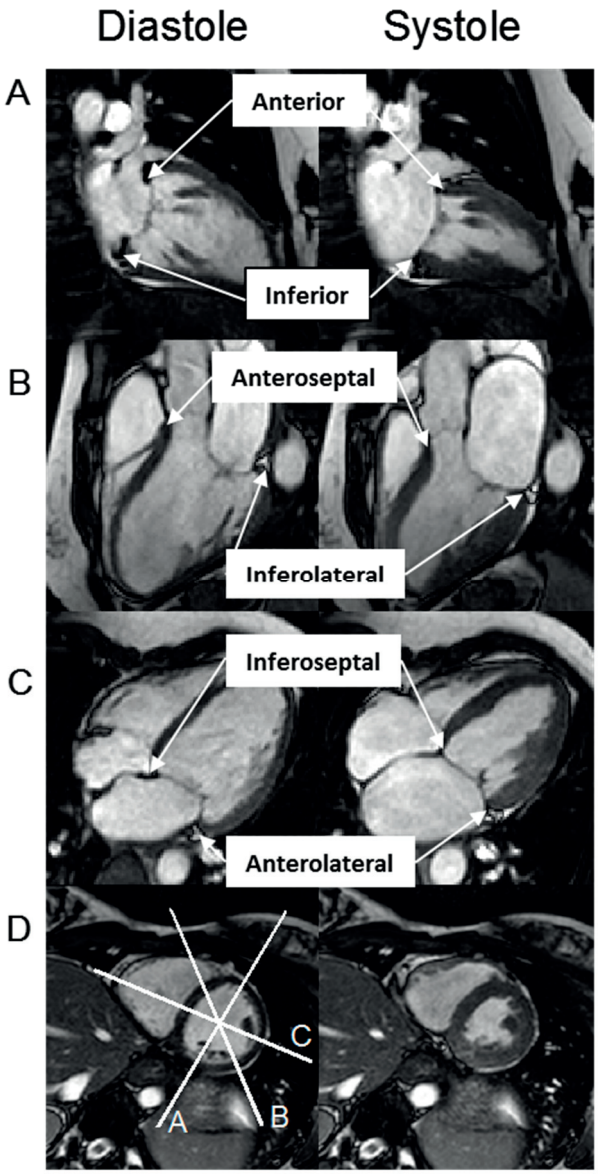

Figure 1.8. Determination of AVPD on SSFP images. A: Anterior and inferior locations in ED and ES in a long-axis 2-chamber image. B: Anteroseptal and inferolateral locations in ED and ES in a long-axis 3-chamber image. C: Anterolateral and inferoseptal locations in a long-axis 4-chamber image. D:Midventricular short-axis image of the LV. The white lines indicate the orientations of the long-axis planes. Adapted from Jonson B, Wollmer P, editors. Klinisk Fysiologi. Stockholm: Liber; 2011

AVPD contribution to SV can be calculated by multiplying AVPD by the epicardial surface area (6)(60). This was first proposed by Lundbäck in 1986 (60). Several studies have shown that AVPD is the main contributor to LV function (28)(31)(32)(33), and it correlates well with EF (62).

Wall thickening is the percent change in radial wall thickness between ES and ED. It is measured in short-axis images and presented in the AHA 17-segment model. Ugander et al. (63) have shown that WT is negatively correlated with infarct transmurality, and that WT is decreased in adjacent myocardial segments. Another study has shown that WT of <30% can be used as a cutoff value to distinguish infarcted from noninfarcted segments after MI (64).

Septal and nonseptal- radial (lateral) contributions to SV were calculated from short-axis solid-state free-precession (SSFP) images. The most basal slice used had a circumferential LV in both ED and ES, and the most apical slice used showed the apex in both ED and ES. Right ventricular (RV) insertion points (2) were manually marked on the epicardial border in both ED and ES. Septal contribution was defined as the percentage of SV generated on the septal side of the RV insertion points, and nonseptal-radial (lateral) was the percent SV generated on the nonseptal side of the RV insertion points.

Strain describes the deformation of an object relative to its original length. Negative strain indicates shortening or compression, and positive strain, lengthening or stretching. Strain, ε, is defined as the change in length (ΔL) in one direction divided by the original length (L_0)

$$\varepsilon = \frac{\Delta L}{L_0}$$

When a material is compressed in one direction, it expands in the perpendicular direction (Figure 1.9).

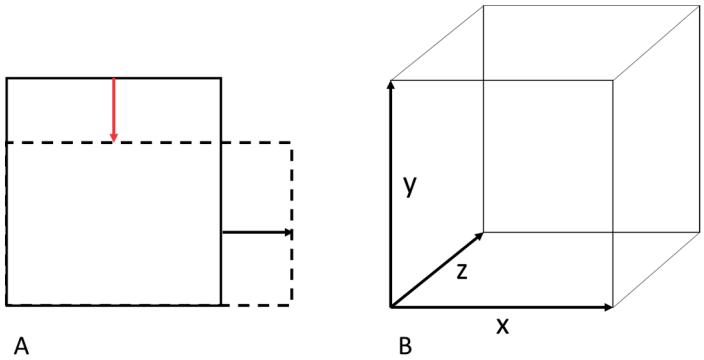

Figure 1.9. Strain. A: 2-dimensional (2D) strain. The grey rectangle with a solid line is the original state, and the rectangle with the broken line the deformed state. The red arrow shows the negative strain in the ”up-down” direction, and the black arrow the positive strain in the ”left-right” direction. B: A cube can be deformed in the x, y, or z direction or in any combined direction (shear strain). Contraction and expansion can occur simultaneously in many directions.

Although strain can be measured in any direction, it is customary to report longitudinal, radial, or circumferential strain in cardiac analysis (65) (Figure 1.10). Shear strain is sometimes also reported. Longitudinal strain is normally reported as negative, reflecting the LV shortening during systole. Regional longitudinal strain increases from apex to base (signifying increased deformation at the base) and is greater in the free wall than in the septum (66). Radial strain is reported as positive due to thickening of the LV wall during systole and is generally greater in the free wall (anterior and lateral) than in the septum in healthy hearts (67) (68). The LV circumference decreases during systole, and circumferential strain is thus normally reported as negative.

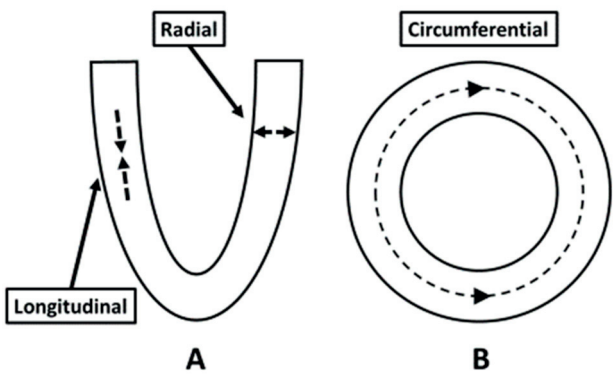

Figure 1.10. A: Illustration of the left ventricular long axis. Arrows indicate longitudinal and radial strain directions. B: Illustration of the left ventricular short axis. Arrows indicate circumferential strain.

Global and regional strain can be measured. Generally, global strain measurements are more dependable than regional strain (69) (70). Changes in regional strain may reveal changes in the myocardium not picked up by global measurements.

In Study 3, strain was determined by measuring the distance from the AV plane to the apex in ED and ES and dividing the difference by the ED distance, as previously described and validated (67).

$$\text{Longitudinal strain} = (\text{Distance in ES} - \text{distance in ED}) / \text{distance in ED}$$

This was done for the anterior, anteroseptal, inferoseptal, inferior, inferolateral, and anterolateral walls of the LV.

CMR-imaging methods to measure strain

Several different CMR-imaging methods are used to measure strain. *Myocardial tagging* (71) is considered the reference method (72). The myocardium is magnetically tagged at the onset of image acquisition and the tags are tracked throughout the cardiac cycle (71). As the tissue deforms, the tags move with the tissue and deformation can be quantified. Signal fading throughout the cardiac cycle is a disadvantage, and postprocessing times may be relatively long. *Phase contrast velocity-encoded strain* (73) measures tissue velocities in 2 or 3 dimensions. A reference scan, such as an SSFP cine image, is obtained and the myocardial contours are manually delineated. A mesh is fit to the myocardial contour. The contour with mesh is placed on the velocity images, and the mesh is deformed by the velocity field. Strain can then be calculated.

Cine-derived strain (74), also called feature tracking, is a newer method that retrospectively tracks edges or contours using SSFP cine images. The method tracks the endocardial border from time frame to time frame and derives strain. It is not reliable when myocardial border definition is indistinct (75) and has lower intra- and interobserver agreement than tagging (76). *Displacement encoding with simulated echoes (DENSE)* (77) and *strain-encoding (SENC)* (78) are 2 other advanced strain methods mainly used in research settings.

“You can’t go back and change the beginning, but you can start where you are and change the end.”

C. S. Lewis

2. Aims

Paper 1: To provide a quantitative and clinically applicable method for calculating strain, and to provide associated normal values for the method.

Paper 2: To investigate how regional myocardial wall function, assessed by CMR-imaging velocity-encoded strain and regional wall thickening, changes after acute myocardial infarction and to find out if we could differentiate between ischemic, adjacent, and remote myocardium as determined by myocardial perfusion study (MPS) by assessing regional myocardial function.

Paper 3: To determine the effects of STEMI on global and regional AVPD, the contribution of AVPD, septal and non-septal radial motion to SV, and to study the relationship between AVPD and infarct size (IS) as well as location.

Paper 4: To investigate the evolution of longitudinal LV function, measured as AVPD, and radial function, measured as WT, globally and regionally from the sub-acute (2-6 days) to the chronic phase (6 months) after STEMI.

"If you're walking down the right path and you are willing to keep walking, eventually you'll make progress."

Barack Obama

3. Materials and methods

Phantom

A U-shaped gelatin phantom was constructed, measuring 100 × 70 × 15 mm, to simulate a slice of the LV. Copper sulfate was added to the gelatin in order to increase the MRI signal and to obtain T1 and T2 relaxation times similar to normal myocardial tissue. A CMR-compatible pneumatic compression device was created to rhythmically compress the phantom 15 mm in the longitudinal direction (Figure 3.1).

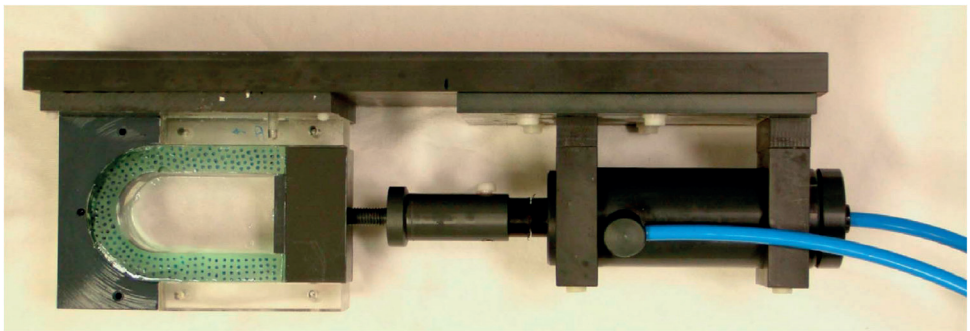

Figure 3.1. Set-up used in phantom experiment..

Phantom experiment

The gelatin phantom was marked with a grid pattern, and 3 regions of interest were identified. The phantom was filmed with a video camera while being rhythmically compressed, simulating LV movement. Custom software was developed to track the optical grid pattern and calculate strain. CMR imaging of the phantom was performed with the same imaging protocol (SSFP cine and TFE strain) as was used in healthy volunteers in Study 1.

Ethical approval

All studies were approved by the Ethical Review Committee at Lund University and complied with the Helsinki declaration. Patients and controls enrolled at Lund signed written informed consent statements. Patients from the CHILL-MI (79) and MITOCARE (80) studies signed written informed consent forms when entering the original study. The animal study complied with the guidelines of the National

Institutes of Health for the care and use of laboratory animals and was approved by the animal research committee at Lund University.

Human studies

In *Study 1*, 36 healthy volunteers were recruited in Lund by advertising and underwent CMR imaging. Exclusion criteria included history of heart disease, hypertension, diabetes, or current pregnancy. Ten patients from a previous study (81) who were examined with CMR imaging 1 week after MI were included for comparison.

Patients from the international multicenter studies CHILL-MI (79) (n=92) and MITOCARE (80) (n=85) were considered for inclusion in *Study 3*. All patients had a first STEMI treated with PCI and had a CMR-imaging study within 1 week. The purpose of CHILL-MI was to study if an infusion of cold saline, given as an adjunct to primary PCI, reduced MI size, but the outcome was negative. MITOCARE evaluated the efficacy and safety of a new drug, TRO40303. Although safe to use, the trial failed to show an effect on the primary endpoint, reduced infarct size. From these studies, 177 patients had satisfactory CMR-imaging data and were included in Study 3. Twenty healthy controls from a previous study were included for comparison (31).

A subset of patients from CHILL-MI (n=88) underwent follow-up CMR imaging 6 months after STEMI and were considered for inclusion in *Study 4*. Eleven patients were excluded due to incomplete data or poor image quality; thus 77 patients were included in Study 4. Twenty healthy controls were included for comparison (31).

Animal study

Ten domestic pigs, weighing 40–50 kg, were anesthetized and underwent a baseline CMR-imaging study. Myocardial ischemia was induced by inflating an angioplasty balloon in the LAD, distal to the diagonal branch, for 40 minutes. An angiogram was performed during inflation to ensure proper placement of the balloon, and 500 MBq of ^{99m}Tc tetrofosmin was administered intravenously 10 minutes before deflation. Another angiogram was performed after deflation to ensure restored blood flow. SPECT was performed 2–-3 hours after reperfusion for identification of the ischemic area, and a second CMR-imaging study was performed 3–4 hours after deflation. Approximately 15 minutes before the acquisition of LGE images, 0.2 mmol/kg of gadolinium contrast was administered intravenously. The animals were euthanized after the second CMR-imaging study.

CMR imaging and analysis

Patients, healthy volunteers, and animals were placed in the supine position, and images were obtained using retrospective ECG gating.

Long-axis SSFP cine images were acquired in 2-, 3-, and 4-chamber views. These images were used for manual delineation of the LV in Papers 1 and 2. In Papers 3 and 4, long-axis SSFP cine images were used for AV-plane analysis. The AV plane was identified and manually indicated in 6 locations during ED and ES (anterior, anteroseptal, inferoseptal, inferior, inferolateral, and anterolateral). The apex was indicated and used as a reference point for AVPD.

Short-axis SSFP cine images covering the LV from base to apex were used in Papers 2, 3, and 4. The epicardial and endocardial LV borders were manually delineated in all time frames. The delineations were used to calculate EDV, end-systolic volume (ESV), SV, left ventricular mass (LVM), WT, and epicardial surface area. In Study 3, RV insertion points were identified and marked on the epicardial border to calculate lateral and non-lateral-septal contributions to SV. The most basal short axis slice included in WT analysis was that showing myocardium in 360° in ED. Midventricular short-axis images were used to determine WT in Study 4. Papillary muscles were excluded.

2D velocity-encoded strain was used in Studies 1 and 2. Velocity data were obtained in 2 directions using the same long-axis planes as the SSFP images. The 2 velocity directions were measured in the same heartbeat. Superior and inferior saturation bands were used. Image resolution was typically 1.5 × 1.5 mm. Figure 3.2 describes the process.

Fast-gradient field echo (FFE) images were collected for about 1 minute during free breathing, collecting 16–22 timeframes during the cardiac cycle.

Turbo-gradient field echo (TFE) images were collected for 15–25 seconds during end-expiratory apnea, collecting 12–16 timeframes during the cardiac cycle.

Late gadolinium enhancement (LGE) was used for infarct quantification. Extracellular space is increased after acute MI due to necrosis and edema, and in chronic infarcts due to scar tissue (82). Since gadolinium contrast is distributed in the extracellular space, infarcted myocardium appears hyperenhanced 10–30 minutes after intravenous administration of gadolinium contrast (83)(84). LGE is considered the reference method for determination of MI size (85)(17). Computer algorithms were used in Studies 2–4 to quantify MI size using LGE (86).

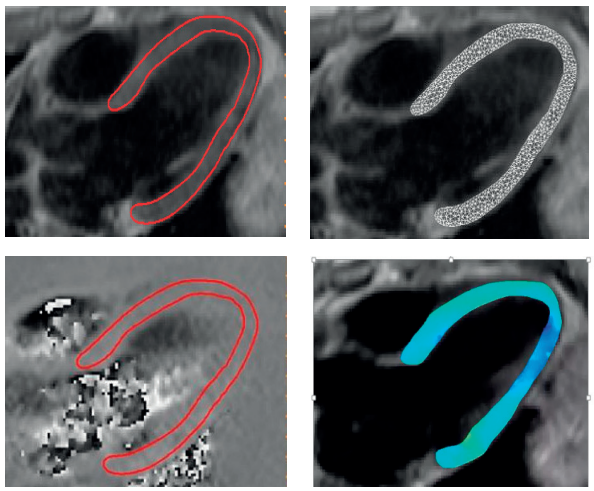

Figure 3.2. Process used to determine 2D velocity strain. Upper left: Manual delineation of the left ventricle was done in the end-diastolic timeframe using long-axis SSFP images. Upper right: The software placed a mesh over the delineated area. Lower left: Delineation and mesh were transferred to the 2D velocity-encoded images, and the myocardial contour was tracked in each timeframe using the acquired velocity data and an optimization algorithm. Lower right: Longitudinal and radial strain were derived. Delineation could be modified in the SSFP images when needed and was automatically transferred to the velocity-encoded images.

MRI scanners

Cardiac magnetic resonance images were acquired on 1.5-T MRI scanners. Philips Intera CV 1.5 T (Philips Medical Systems, Best, the Netherlands) was used in Studies 1 and 2. In Studies 3 and 4, patients from multicenter studies were included, and images from Siemens Healthcare, GE Healthcare, and Philips Medical Systems MRI scanners were used.

Ischemic, adjacent, and remote myocardium

In Study 2, LV segments were classified according to the degree of ischemia detected on SPECT. Using the AHA 17-segment model, segments with counts <50% were classified as ischemic, segments with counts of 51%–99% were classified as adjacent, and segments with normal counts were classified as remote. An example is shown in Figure 1.7. Figure 3.3 illustrates typical infarct distribution after the occlusion of the respective coronary artery. There is, however, significant variation and overlap.

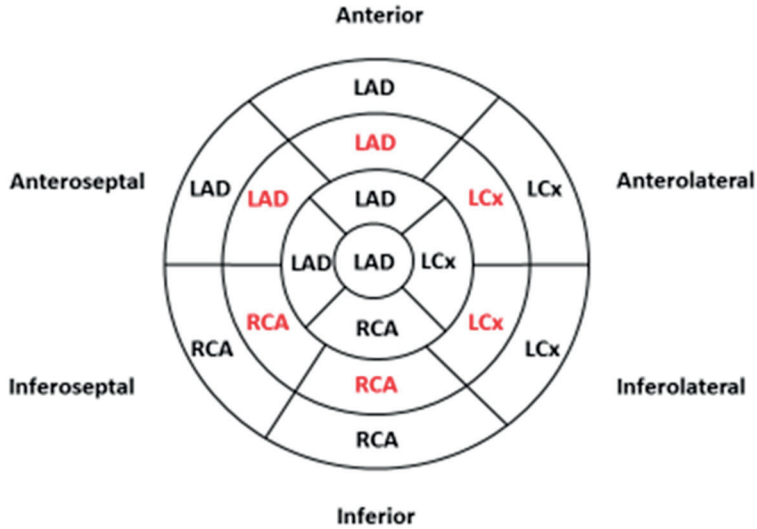

Figure 3.3. Typical infarction patterns after occlusion of the left anterior descending (LAD), right coronary artery (RCA), and left circumflex (LCx) coronary arteries. Red indicates mid-ventricular segments.

Mid-ventricular segments were used in Study 4 for WT analysis (Figure 3.3). We considered anterior and anteroseptal segments ischemic; inferoseptal and anterolateral segments adjacent, and inferior and inferolateral segments remote for patients with LAD occlusion. For patients with RCA occlusion, inferoseptal and inferior segments were considered infarcted, anteroseptal and inferolateral segments considered adjacent, and anterolateral and anterior segments remote. For patients with LCx occlusion, we considered the inferolateral and anterolateral segments ischemic, the inferior and anterior segments adjacent and the anteroseptal and inferoseptal remote.

Myocardial salvage index (MSI) was defined as 1 – (infarct size by LGE)/(ischemic volume by MPS) in a similar fashion as described earlier (81)(87).

Statistics

Continuous variables were presented as mean ± SD. Results with a p-value<0.05 were considered statistically significant. For normally distributed data, paired or unpaired Student's *t* test was performed. The Wilcoxon signed-rank test was used when the population was small and normal distribution of the data could not be assumed. Bland-Altman analysis was used in Study 1 to compare results from optical tracking and velocity-encoded strain. The Pearson coefficient of correlation

was used in Studies 1 and 4. In Study 4, the difference between correlation coefficients was computed using the *r*-to-Fisher-*z* transformation. ROC analysis was performed in Study 2 to discriminate between ischemic, adjacent, and remote areas of myocardium. Sensitivities and specificities for the best thresholds were reported. Linear regression analysis was performed in Study 3 to determine the correlation between infarct and functional parameters. One-way analysis of variance (ANOVA) with the Tukey post-hoc test was used to compare results between patients with LAD, RCA, and LCx infarcts. Inter- and intraobserver variabilities were calculated by taking the difference between Observers 1 and 2 (Study 1 and Study 3). Mean (bias) and standard deviation (variability) were calculated, and in Study 3, intraclass correlation (ICC) was calculated. Internal validation of the "contributions to SV" was obtained in Study 3 by adding AVPD, septal, and nonseptal radial contributions to SV for each subject where the result ideally would add up to 100% of SV.

"The truth is rarely pure and never simple."

Oscar Wilde

4. Results and discussion

Validation of 2D velocity-encoded strain and normal values (Study 1)

Validation of 2D-velocity encoded strain

Results from the phantom experiment are presented in Figures 4.1 and 4.2. There was excellent agreement between CMR velocity-encoded strain (TFE) and optical tracking and only small bias (0.0025 ± 0.085).

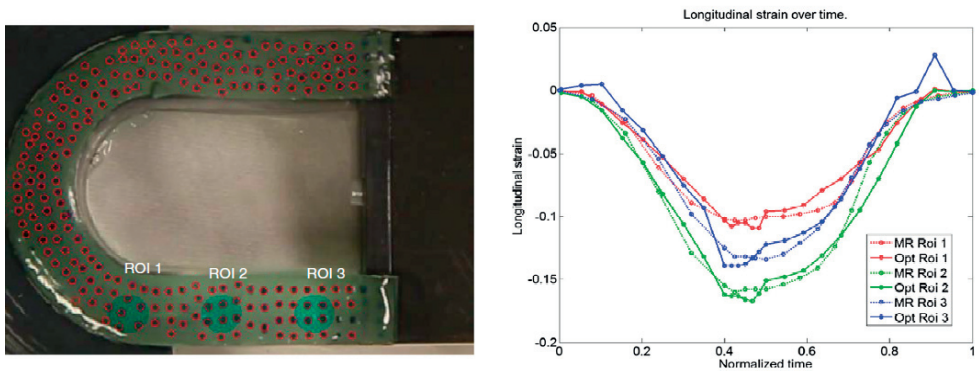

Figure 4.1. Optical tracking and velocity-encoded strain (TFE) for 3 regions of interest (ROI). Each color represents a region of interest. MR = velocity-encoded strain measurement using CMR, Opt = optical measurement.

TFE vs. FFE

After validation of velocity-encoded strain in the phantom model, we proceeded to investigate whether TFE or FFE velocity-encoded strain images were best suited for further analysis by testing intra- and interobserver variability. Intraobserver variability for longitudinal strain was lower for TFE (0.00 ± 0.06) than for FFE (−0.01 ± 0.11), and this was thought to be due to artifacts caused by breathing motion during FFE. We performed no further analysis of FFE images as they were felt to be inferior. We found greater intraobserver variability for the basal segments, and this was attributed to their more complex motion. The intraobserver variability was very high for radial strain (0.10 ± 0.33).

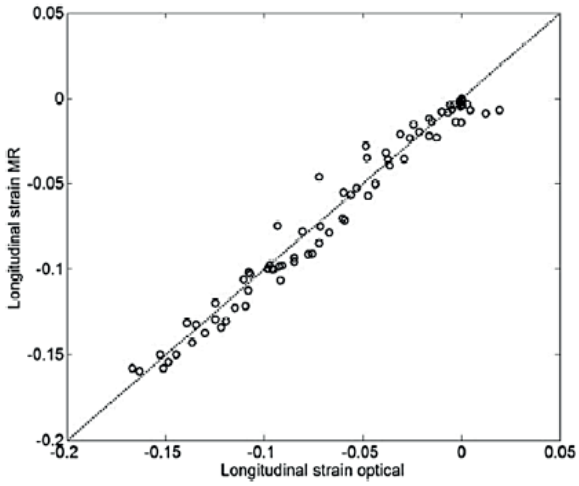

Figure 4.2. Relationship between optical tracking and longitudinal velocity-encoded strain from CMR. The dashed line indicates the line of identity.

Velocity-encoded strain in healthy volunteers

We used TFE images in further analysis and found global longitudinal strain of -0.18 ± 0.10 in healthy volunteers. We found no correlation between global longitudinal strain and age (r^2 = 0.097, p=ns). Figure 4.3 shows typical longitudinal strain pattern in a healthy volunteer.

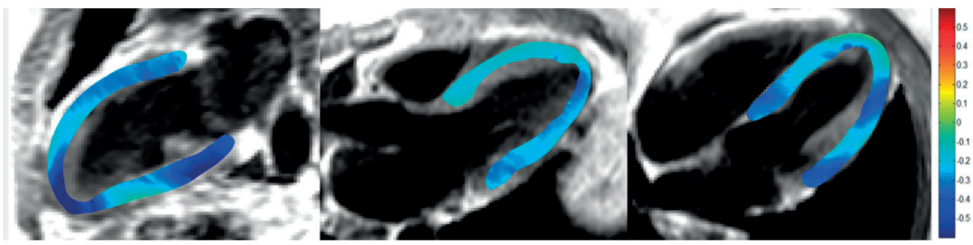

Figure 4.3. Typical longitudinal strain pattern in a healthy volunteer. Left: 2-chamber view. Middle: 3-chamber view. Right: 4-chamber view.

Velocity-encoded strain in patients after MI

Patients had lower mean global longitudinal strain (-0.15 ± 0.1) than did healthy volunteers (p<0.05). Figure 4.4 shows longitudinal strain in a patient after MI.

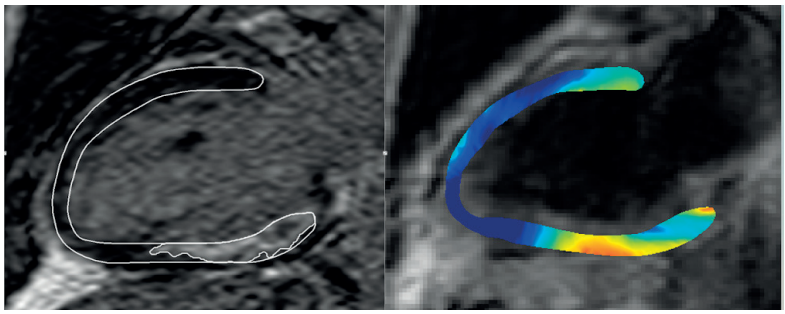

Figure 4.4. Longitudinal strain in patient after myocardial infarction. Left: late gadolinium enhancement image. The lighter area that is delineated is the infarct. Right: decreased strain in the area of the infarct.

We validated velocity-encoded strain against optical measurements in the phantom experiment. TFE had lower intra- and interobserver variability than FFE, probably because of breathing-motion ghost artifacts in the FFE images. Intraobserver variability was high for radial strain, and this was attributed to the large voxel size (1.5 mm) in relation to typical wall thickening (2–4 mm); therefore, we did not present any data on radial strain. Global longitudinal strain found in healthy volunteers (-0.18) was similar to findings by Moore (-0.16) (68) and Bogaert (-0.17) (88) and was significantly lower in patients (-0.15; $p<0.05$). Patients had decreased function in both infarcted and remote regions (60% ± 27% in infarcted regions vs. 88 ± 27% in remote). Mean segmental longitudinal strain for the healthy volunteers is presented in Figure 4.5.

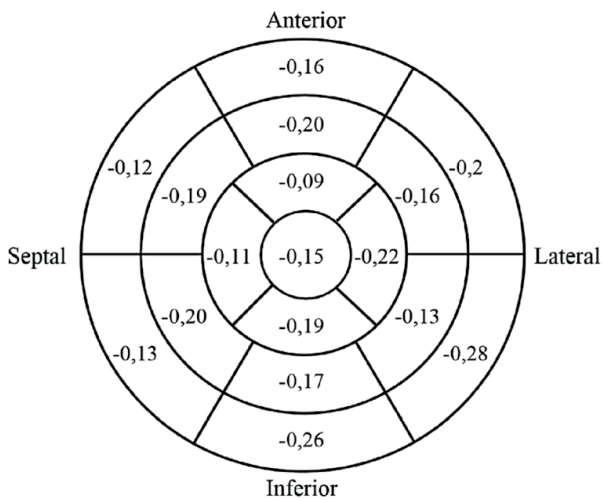

Figure 4.5. Mean longitudinal strain in healthy volunteers presented in the AHA 17-segment model.

LV function in the hyper-acute phase of ischemia (Study 2)

2D velocity-encoded strain TFE and SSFP cine images were obtained in 10 pigs at baseline and after 40-minute occlusion of the LAD. Left ventricular segments were classified as ischemic, adjacent, or remote based on SPECT results.

Longitudinal strain before and after ischemia

Mean longitudinal strain was decreased in ischemic and adjacent segments ($p<0.001$ for both) after ischemia compared with baseline. There was no change in mean longitudinal strain in remote segments compared with baseline (Figure 4.6).

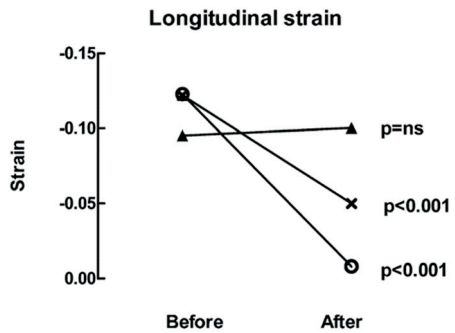

Figure 4.6. Mean longitudinal strain in ischemic (**o**), adjacent (**x**), and remote (▲) segments before and after ischemia in 10 pigs.

Radial strain before and after ischemia

Mean radial strain was decreased in ischemic and adjacent segments after ischemia ($p<0.001$ for both), and mean radial strain was increased in remote segments ($p<0.002$), compared with baseline ($p<0.05$; Figure 4.7).

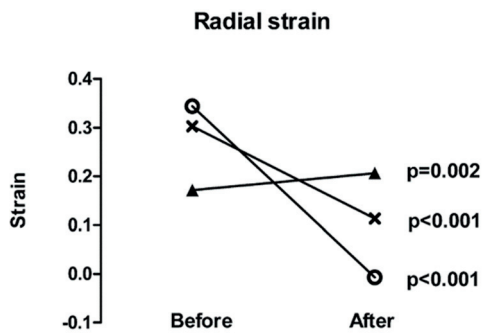

Figure 4.7. Mean radial strain in ischemic (**o**), adjacent (**x**), and remote (▲) segments before and after ischemia in 10 pigs.

Wall thickening before and after ischemia

Mean WT was decreased in ischemic and adjacent segments ($p<0.001$ for both) and was increased in remote myocardial segments ($p<0.01$; Figure 4.8). As expected, there was a strong correlation between mean WT and mean radial strain ($r = 0.86$; $p<0.001$).

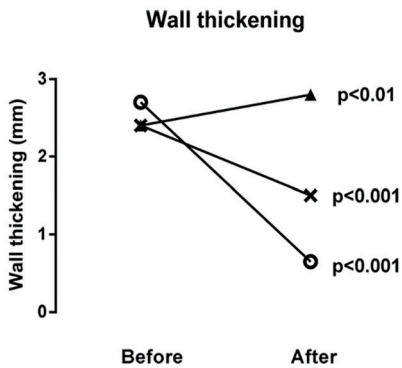

Figure 4.8. Wall thickening in ischemic (**o**), adjacent (**x**), and remote (▲) segments before and after ischemia.

Thresholds for ischemic, adjacent, and remote myocardium

ROC analysis was performed to find thresholds to differentiate between ischemic, adjacent, and remote myocardium for WT, radial strain, and longitudinal strain. Table 4.1 presents the thresholds found to discriminate best.

Table 4.1. Thresholds for wall thickening, radial strain, and longitudinal strain determined by ROC analysis for differentiations between ischemic, adjacent, and remote myocardium.

	Threshold	Sensitivity%	Specificity%
Wall thickening ischemic	< 1.4 mm	80	76
Wall thickening adjacent	1.4 - 2.1 mm	35	90
Wall thickening remote	>2.1 mm	76	81
Radial strain ischemic	< 0.06	77	77
Radial strain adjacent	0.06-0.15	33	89
Radial strain remote	>0.15	73	77
Long. strain ischemic	> –0.04	70	72
Long. strain adjacent	–0.04 - -0.07	15	88
Long. strain remote	<–0.07	73	71

In this experimental study in the hyperacute phase (3-4 hours) after ischemia, we found dramatically decreased LV function in ischemic and adjacent areas, and preserved or increased function in remote areas. Reduced function in the ischemic areas can be attributed to the direct ischemic insult and to the presence of edema (37% ± 3% increase in LVM after ischemia in ischemic area) (89). The decrease in adjacent areas is likely due to stunning that can persist for hours to weeks after ischemia (90). The sensitivities and specificities for the best thresholds to identify ischemic myocardium was 80% and 76% for WT, 77% and 77% for radial strain, and 70% and 72% for longitudinal strain, respectively. Sensitivities and specificities were lower for adjacent and remote myocardium. The thresholds have limited applicability due to the low sensitivity and specificity.

Longitudinal LV function within a week of STEMI (Study 3)

AVPD

Mean global AVPD was decreased in patients within a week of STEMI (11 ± 2 mm) compared with controls (15 ± 2; $p<0.001$). There were significant decreases in walls with and without infarction (Figure 4.9, Table 4.2).

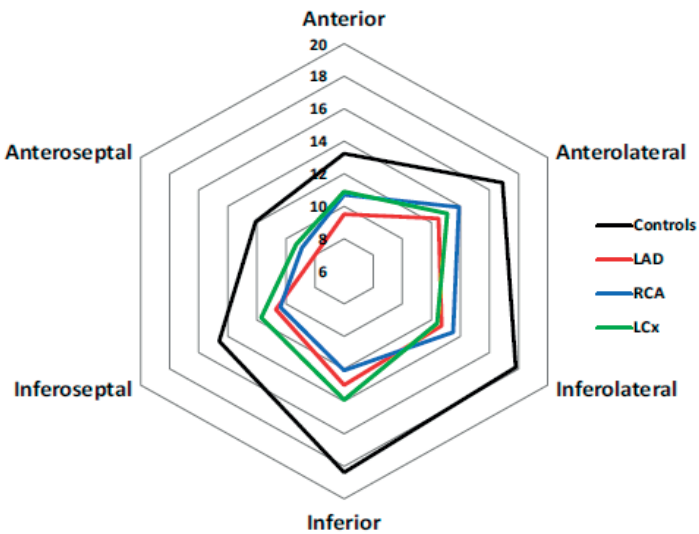

Figure 4.9. Mean AVPD for each LV wall in millimeters. Black line = controls, red line = LAD, blue line = RCA, green line = LCx.

Table 4.2. Mean atrioventricular plane displacement (AVPD) (mm) was decreased in patients with left anterior descending (LAD), right coronary artery (RCA), and left circumflex (LCx) infarcts compared with controls (p<0.001 for all).

	Anterior	Anteroseptal	Inferoseptal	Inferior	Inferolateral	Anterolateral	LVAVPD
LAD	10 ± 3	8 ± 3	11 ± 3	13 ± 3	13 ± 3	13 ± 3	11 ± 2
RCA	11 ± 3	9 ± 3	10 ± 2	12 ± 3	13 ± 3	14 ± 3	12 ± 2
LCx	11 ± 2	9 ± 2	12 ± 2	14 ± 3	12 ± 3	13 ± 33	12 ± 2
Controls	13 ± 2	12 ± 2	15 ± 1	18 ± 2	18 ± 2	17 ± 2	15 ± 2

Global AVPD did not differ in patients with LAD, RCA, or LCx infarction (p=0.18). We found a weak negative correlation between IS and decreased AVPD (R^2=0.06, p<0.001; Figure 4.10).

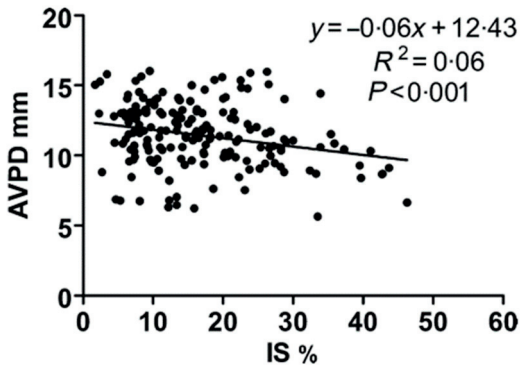

Figure 4.10. Relationship between atrioventricular plane displacement (AVPD) (mm) and infarct size (IS; percent infarcted myocardium of total left ventricular mass).

Longitudinal strain

Mean global longitudinal strain was decreased in patients (-0.14 ± 0.05) compared to controls (-0.17 ± 0.04; p<0.001). Regional longitudinal strain was decreased in all LV segments (Table 4.3).

Table 4.3. Regional longitudinal strain for patients and controls. P< 0.001 for all except the anterolateral wall in patients with LCx infarcts (p<0.01).

	Anterior	Anteroseptal	Inferoseptal	Inferior	Inferolateral	Anterolateral
LAD	−0·10 ± 0·03	−0·09 ± 0·03	−0·11 ± 0·03	−0·13 ± 0·03	−0·13 ± 0·03	−0·12 ± 0·02
RCA	−0·12 ± 0·03	−0·11 ± 0·03	−0·12 ± 0·02	−0·13 ± 0·03	−0·15 ± 0·03	−0·14 ± 0·02
LCx	−0·11 ± 0·02	−0·11 ± 0·04	−0·12 ± 0·02	−0·14 ± 0·04	−0·13 ± 0·03	−0·13 ± 0·03
Controls	−0·14 ± 0·02	−0·14 ± 0·02	−0·16 ± 0·02	−0·19 ± 0·03	−0·19 ± 0·03	−0·17 ± 0·04

Contribution to SV

AVPD contribution to SV was lower in patients (58% ± 9%) than in controls (64% ± 8%; $p<0.001$). The septal and non-septal radial contributions to SV were similar in patients and controls except for an increased septal contribution in LCx patients. Adding AVPD, septal, and non-septal radial contributions to SV accounted for 99% ± 9% of SV for patients and 103% ± 9% for controls.

Decreased longitudinal function (AVPD and longitudinal strain) seen in infarcted areas is attributable to the ischemic injury resulting in edema, necrosis, and postischemic stunning (90). Decreases in surrounding and remote areas may be due to the global inflammatory response, with inflammation and changes in contractile and mitochondrial proteins described after STEMI (91). Medications such as beta-blockers, often prescribed to patients after MI, may also contribute to the global decrease of longitudinal function. Finally, the different parts of the LV are all connected at the fibrous AV plane, and reduced AVPD in one area may influence the entire movement of the AV plane (92).

The global decrease in longitudinal function within a week of STEMI is why it is difficult to determine MI location visually using longitudinal measures (93). This is in line with Rosendahl et al., who found a rather low sensitivity of 64% using longitudinal strain (echocardiography) to detect infarction with 80% specificity (94). Støylen et al. have also shown inability to localize the infarction from AVPD measurements in 19 MI patients using echocardiography (95). The global decrease in longitudinal function can also explain why Rangarajan et al. found that lateral MAPSE alone is an independent predictor of major adverse cardiac events (93).

Evolution of LV function after STEMI (Study 4)

AVPD

Global AVPD was decreased in the subacute (12 ± 2 mm) and chronic (13 ± 2 mm) phases after STEMI compared with controls (15 ± 2 mm; $p<0.001$ for both), with partial recovery in the chronic phase.

Patients with an LAD (n= 28) or RCA infarct (n=39) had decreased AVPD in both infarcted and remote segments in the subacute and chronic phases after STEMI (Figure 4.11, upper and middle panels, respectively). Patients with an LCx infarct (n=10) had decreased AVPD in all but one remote segment (anterior) in the subacute phase (Figure 4.11, lower panel). This decrease remained significant only in 2 segments (inferolateral and inferoseptal) in the chronic phase after STEMI).

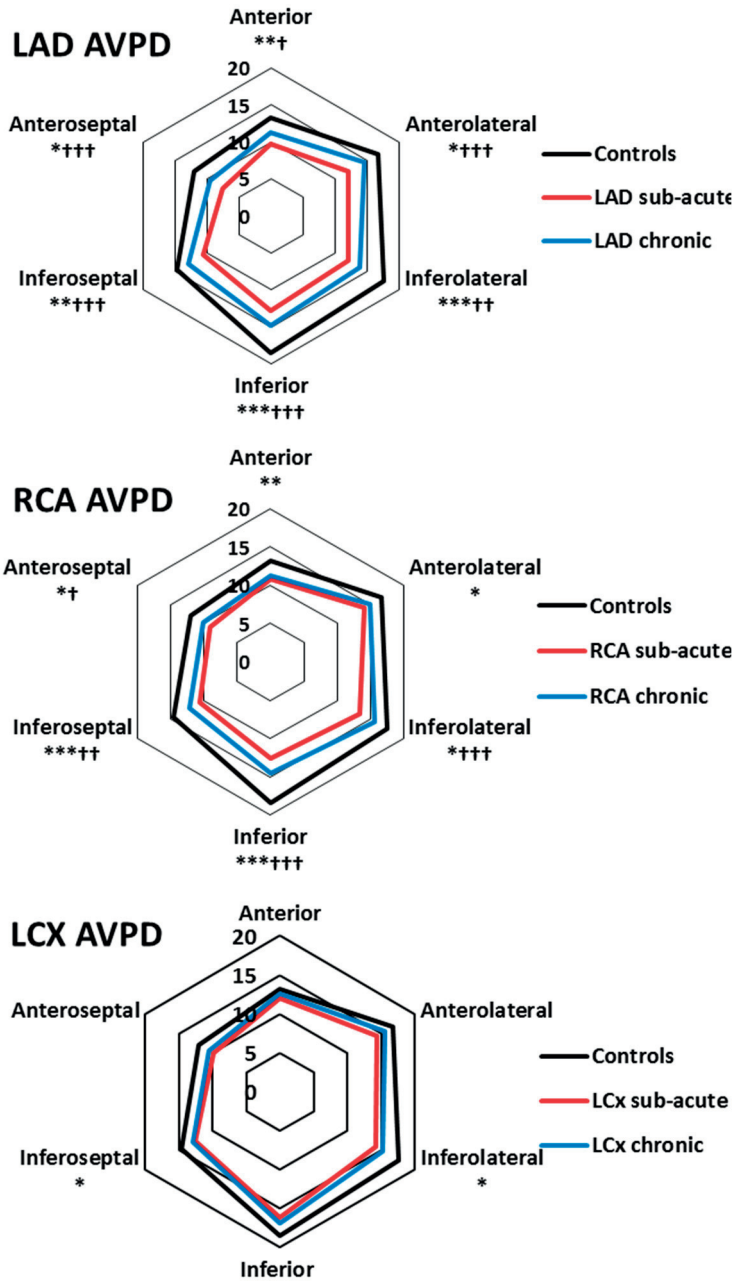

Figure 4.11. AVPD in mm according to culprit vessel. Black lines represent controls, red lines patients in the sub-acute phase, and blue lines patients in the chronic phase after STEMI. Upper: patients with infarction in the LAD territory. Middle: patients with infarction in the RCA territory. Lower: Patients with infarction in the LCx territory. Comparisons between the chronic phase after STEMI and controls: *p<0.05. **p<0.01. ***p<0.001. Comparisons between the subacute and chronic phases after STEMI: †p<0.05. ††p<0.01. †††p<0.001.

Contribution to SV

The relative contribution of AVPD to SV was decreased in patients in the subacute phase (59%; p<0.01) and chronic phase (58%; p<0.05) compared with controls (64%).

Segmental WT

Mean segmental WT was decreased in all LV segments in patients with LAD infarction in the subacute and chronic phases after STEMI compared with controls. The decrease was most prominent in the anterolateral, anterior, anteroseptal, and inferoseptal segments. Partial recovery was seen in these segments after 6 months.

Table 4.4. Evolution of segmental WT after STEMI

	Anterior	Anteroseptal	Inferoseptal	Inferior	Inferolateral	Anterolateral
Controls (n=20)	71 ± 25	65 ± 22	59 ± 18	72 ± 22	79 ± 30	75 ± 25
LAD Subacute (n=28)	I 27 ± 17 ***	1 18 ± 15 ***	A 31 ± 15 ***	R 53 ± 17 **	R 54 ± 23 **	A 42 ± 20 ***
LAD Chronic (n=28)	I 47 ± 34 * †††	I 42 ± 27 * †††	A 46 ± 18 * †††	R 60 ± 15 *	R 62 ± 16 *	A 53 ± 24 ** ††
RCA Subacute (n=39)	R 70 ± 21	A 64 ± 19	I 40 ± 13 ***	I 34 ± 18 ***	A 47 ± 21 ***	R 56 ± 21 **
RCA Chronic (n=39)	R 71 ± 20	A 64 ± 20	I 43 ± 18 **	I 46 ± 23 *** †††	A 58 ± 24 ** †††	R 63 ± 20 †
LCx Subacute (n=10)	R 63 ± 21	R 63 ± 12	A 51 ± 15 **	I 37 ± 20 ***	I 36 ± 20 ***	A 46 ± 19 **
LCx chronic (n=9)	R 89 ± 21 †	R 80 ± 11 †	A 54 ± 13	I 56 ± 14 ††	I 51 ± 22 *	A 60 ± 21

A = adjacent segments; I = ischemic segments; R = remote segments. Comparison between patients and controls: *p<0.05. **p<0.01. ***p<0.001. Comparison between patients 1 week and 6 months after STEMI: †p<0.05. ††p<0.01. †††p<0.001.

Patients with RCA infarcts had decreased WT in inferoseptal, inferior, inferolateral and anterolateral LV segments in the sub-acute phase with recovery of function in the anterolateral segment and partial recovery in inferior and inferolateral segments. Patients with LCx infarcts had decreased WT in the inferior, inferolateral and anterolateral segments in the sub-acute phase. One patient in this group did not have short axis CMR images in the chronic phase and was therefore excluded from WT

analysis in this phase. WT remained decreased only in the inferolateral segment in the chronic phase.

The mean global AVPD found in controls in Studies 3 and 4 (15 ± 2 mm for both) is similar to results by Støylen *et al.* who found a MAPSE of 16 mm using echocardiography (95). Støylen also reported MAPSE of 12 mm within a week of MI and we found it to be 12 mm in the sub-acute and 13 mm in the chronic phases after STEMI.

The widespread decrease in AVPD seen in the chronic phase after STEMI suggests that it remains difficult to differentiate between infarcted and noninfarcted myocardium using longitudinal measures even in this phase. The global effect on longitudinal function caused by regional ischemic injury has several possible explanations. The LV walls and cardiac valves are attached to the fibrous and somewhat stiff AV plane, and this prohibits large regional differences in movement between parts of the plane (92). Another explanation is that remote myocardium is not unaffected by STEMI: inflammatory cells that affect mitochondrial proteins (91), and expansion of extra cellular volume have been found also in remote myocardium (96). Finally, the use of medications in the chronic phase after STEMI, such as beta-blockers, may also affect the myocardium globally.

The challenge when using WT to identify MI location is thus not only that the change in radial thickness is quite small and can be difficult to quantify visually but also that both infarcted and remote myocardium have decreased WT in large LAD infarcts. Recently, Everaars et al. showed that strain from tagging CMR was superior to WT when identifying infarcted and remote myocardium (97).

The timing of myocardial recovery after STEMI is debated. Ingul et al. found that most of the systolic function was regained within the first 2 days after STEMI (98). Engblom *et al*. also found an increase in radial WT between Days 1 and 7 after MI but further increases at follow-up 6 and 12 months after the MI (99). Further, Hassell *et al.* recently showed that LV remodeling is an ongoing process for at least 2 years after STEMI (100). In our study, the subacute CMR imaging was performed 2–6 days after STEMI, and it is likely that LV function had partially recovered considering these previous results. However, both longitudinal and radial function significantly improved between the subacute and chronic phases, although function did not reach that of the controls.

"Lead me, follow me, or get out of my way."

General George S. Patton, Jr.

5. Conclusions

Study 1

We presented and validated a robust and clinically applicable technique to quantify longitudinal strain and regional myocardial wall function with associated normal values.

Study 2

Differentiation thresholds for wall thickening and velocity-encoded strain could be established to distinguish between ischemic, adjacent, and remote segments, but they will have limited applicability due to low sensitivity and specificity. There was slight increase in radial strain in remote segments after ischemia. Edema was present mainly in the ischemic region but also in the adjacent and remote segments.

Study 3

Patients have significantly decreased global and regional AVPD within 1 week after STEMI, even in myocardium remote from the infarct. The global AVPD decrease is independent of MI location, and MI size has only a minor effect on the degree of AVPD decrease. Longitudinal contribution is slightly lower than in controls but remains the main contributor to SV even after MI. These results highlight the difficulty in determining infarct location and size from longitudinal measures of LV function.

Study 4

Assessment of regional longitudinal and radial function after STEMI is complex. Decrease in regional function can be seen in segments without infarction, even in the chronic phase. This information is important to consider when the combination of functional and infarct quantification is used for diagnosis of post-ischemic stunning and hibernation.

Interpretation of regional function after myocardial infarction may seem to be straightforward, but our studies have showed the complexity of both longitudinal and radial measures. In Study 2, we showed the difficulty in finding clinically useful thresholds for regional function that can differentiate between infarcted, adjacent, and remote myocardium with velocity-encoded strain. This can be explained by the results from Studies 3 and 4, where regional function also was decreased in remote myocardium both in the subacute and chronic phases.

Strain is a widely used technique due to the development of speckle-tracking echocardiography and feature-tracking CMR imaging. Our studies suggests that global measurements of strain may contain information but that regional strain measurements after MI should be used cautiously for determining infarct location or size. The simplicity of AVPD measurements without need for postprocessing, and the previously shown strong prognostic value make it a compelling method for further use.

“If you have a problem cut it in half.”

Jonathan Webb

References

1. WHO. The top 10 causes of death: Fact sheet N°310. World Health Organisation. 2013.
2. Ibanez B, James S, Agewall S, Antunes MJ, Bucciarelli-Ducci C, Bueno H, et al. 2017 ESC Guidelines for the management of acute myocardial infarction in patients presenting with ST-segment elevation. Eur Heart J. 2017;39(2):119–77.
3. Mozaffarian D, Benjamin EJ, Go AS, Arnett DK, Blaha MJ, Cushman M, et al. Executive summary: Heart disease and stroke statistics-2016 update: A Report from the American Heart Association. Circulation. 2016;133(4):447–54.
4. Townsend N, Wilson L, Bhatnagar P, Wickramasinghe K, Rayner M, Nichols M. Cardiovascular disease in Europe: Epidemiological update 2016. Vol. 37, Eur Heart J. 2016. p. 3232–45.
5. Jernberg T. Swedeheart Annual report 2015. Karolinska Univeristy Hosp Huddinge, Stockholm. 2016; Available from: http://www.ucr.uu.se/swedeheart/arsrapport-2017/aeldre-arsrapporter-older-reports/arsrapport-2015
6. Kristensen SD, Laut KG, Fajadet J, Kaifoszova Z, Kala P, Di Mario C, et al. Reperfusion therapy for ST elevation acute myocardial infarction 2010/2011: Current status in 37 ESC countries. Eur Heart J. 2014;35(29):1957–70.
7. Windecker S, Kolh P, Alfonso F, Collet JP, Cremer J, Falk V, et al. 2014 ESC/EACTS Guidelines on myocardial revascularization: The Task Force on Myocardial Revascularization of the European Society of Cardiology (ESC) and the European Association for Cardio-Thoracic Surgery (EACTS). Eur Heart J. 2014;35(37):2541–619.
8. Mozaffarian D, Benjamin EJ, Go AS, Arnett DK, Blaha MJ, Cushman M, et al. Heart disease and stroke statistics-2016 update a report from the American Heart Association. Vol. 133, Circulation. 2016. p. 38–48.
9. Ponikowski P, Voors AA, Anker SD, Bueno H, Cleland JGF, Coats AJS, et al. 2016 ESC Guidelines for the diagnosis and treatment of acute and chronic heart failure. Eur Heart J. 2016;37(27):2129–200.
10. Mosterd A, Hoes AW. Clinical epidemiology of heart failure. Vol. 93, Heart. 2007. p. 1137–1146. Review.
11. Redfield MM, Jacobsen SJ, Burnett JC, Mahoney DW, Bailey KR, Rodeheffer RJ. Burden of systolic and diastolic ventricular dysfunction in the community: Appreciating the scope of the heart failure epidemic. J Am Med Assoc. 2003;289(2):194–202.
12. Maggioni AP, Dahlström U, Filippatos G, Chioncel O, Leiro MC, Drozdz J, et al. EURObservational Research Programme: Regional differences and 1-year follow-up results of the Heart Failure Pilot Survey (ESC-HF Pilot). Eur J Heart Fail. 2013;15(7):808–17.
13. Pennell DJ. Ventricular Volume and Mass by CMR. J Cardiovasc Magn Reson. 2003;4(4):507–13.
14. Gonzalez JA, Kramer CM. Role of imaging techniques for diagnosis, prognosis and management of heart failure patients: Cardiac magnetic resonance. Curr Heart Fail Rep. 2015;12(4):276–83.

15. Maceira AM, Prasad SK, Khan M, Pennell DJ. Normalized left ventricular systolic and diastolic function by steady state free precession cardiovascular magnetic resonance. J Cardiovasc Magn Reson. 2006;8(3):417–26.
16. Messroghli DR, Bainbridge GJ, Alfakih K, Jones TR, Plein S, Ridgway JP, et al. Assessment of regional left ventricular function: Accuracy and reproducibility of positioning standard short-axis sections in cardiac MR imaging. Radiology. 2005;235(1):229–36.
17. Simonetti OP, Kim RJ, Fieno DS, Hillenbrand HB, Wu E, Bundy JM, et al. An Improved MR Imaging Technique for the Visualization of Myocardial Infarction. Radiology. 2001;218(1):215–23.
18. Greenbaum RA, Ho SY, Gibson DG, Becker AE, Anderson RH. Left ventricular fibre architecture in man. Heart. 1981;45(3):248–63.
19. Nordlund D, Heiberg E, Carlsson M, Frund ET, Hoffmann P, Koul S, et al. Extent of myocardium at risk for left anterior descending artery, right coronary artery, and left circumflex artery occlusion depicted by contrast-enhanced steady state free precession and T2-weighted short tau inversion recovery magnetic resonance imaging. Circ Cardiovasc Imaging. 2016;9(7):pii: e004376.
20. Ingels NB. Myocardial fiber architecture and left ventricular function. Technol Health Care. 1997;5(1–2):45–52.
21. Nielles-Vallespin S, Khalique Z, Ferreira PF, de Silva R, Scott AD, Kilner P, et al. Assessment of Myocardial Microstructural Dynamics by In Vivo Diffusion Tensor Cardiac Magnetic Resonance. J Am Coll Cardiol. 2017;69(6):661–76.
22. Helle-Valle T, Crosby J, Edvardsen T, Lyseggen E, Amundsen BH, Smith HJ, et al. New noninvasive method for assessment of left ventricular rotation: speckle tracking echocardiography. Circulation. 2005;112(20):3149–56.
23. Buckberg GD, Mahajan A, Jung B, Markl M, Hennig J, Ballester-Rodes M. MRI myocardial motion and fiber tracking: a confirmation of knowledge from different imaging modalities. Eur J Cardio-thoracic Surg. 2006;29(Suppl. 1):165–77.
24. Ugander M, Carlsson M, Arheden H. Short-axis epicardial volume change is a measure of cardiac left ventricular short-axis function, which is independent of myocardial wall thickness. Am J Physiol Heart Circ Physiol. 2010;298(2):530–5.
25. Carlsson M, Cain P, Holmqvist C, Stahlberg F, Lundback S, Arheden H. Total heart volume variation throughout the cardiac cycle in humans. Am J Physiol Heart Circ Physiol. 2004 Jul 1;287(1):243–50.
26. Slager CJ, Hooghoudt TEH, Serruys PW, Schuurbiers JCH, Reiber JHC, Meester GT, et al. Quantitative assessment of regional left ventricular motion using endocardial landmarks. J Am Coll Cardiol. 1986;7(2):317–26.
27. McDonald IG. The Shape and Movements of the Human Left Ventricle During Systole. Vol. 26, American Journal of Cardiology. 1970. p. 221–30.
28. Carlsson M, Ugander M, Mosén H, Buhre T, Arheden H. Atrioventricular plane displacement is the major contributor to left ventricular pumping in healthy adults, athletes, and patients with dilated cardiomyopathy. Am J Physiol Heart Circ Physiol. 2007 Mar 1;292(3):1452–9.

29. Stephensen S, Steding-Ehrenborg K, Munkhammar P, Heiberg E, Arheden H, Carlsson M. The relationship between longitudinal, lateral, and septal contribution to stroke volume in patients with pulmonary regurgitation and healthy volunteers. Am J Physiol Heart Circ Physiol. 2014;306(6):895–903.
30. Steding-Ehrenborg K, Boushel RC, Calbet JA, Akeson P, Mortensen SP. Left ventricular atrioventricular plane displacement is preserved with lifelong endurance training and is the main determinant of maximal cardiac output. J Physiol. 2015;593(23):5157–66.
31. Asgeirsson D, Hedström E, Jögi J, Pahlm U, Steding-Ehrenborg K, Engblom H, et al. Longitudinal shortening remains the principal component of left ventricular pumping in patients with chronic myocardial infarction even when the absolute atrioventricular plane displacement is decreased. BMC Cardiovasc Disord. 2017;17(1):208.
32. Carlsson M, Ugander M, Heiberg E, Arheden H. The quantitative relationship between longitudinal and radial function in left, right, and total heart pumping in humans. Am J Physiol Heart Circ Physiol. 2007 Jul 1;293(1):636–44.
33. Stephensen SS, Steding K, Arheden H, Heiberg E, Carlsson M. Quantification of the contribution of septal movement to stroke volume in healthy subjects, athletes, patients with pulmonary insufficiency and patients with pulmonary hypertension. J Cardiovasc Magn Reson. 2012;14(Suppl 1):87.
34. What are the signs and symptoms of coronary heart disease? 2015. Available from: https://www.nhlbi.nih.gov/heath-topics/coronary-heart-disease
35. Roffi M, Patrono C, Collet J-P, Mueller C, Valgimigli M, Andreotti F, et al. 2015 ESC Guidelines for the management of acute coronary syndromes in patients presenting without persistent ST-segment elevation. Eur Heart J. 2016;37(3):267–315.
36. Thygesen K, Alpert JS, Jaffe AS, Chaitman BR, Bax JJ, Morrow DA, et al. Fourth universal definition of myocardial infarction (2018). Eur Heart J. 2018;1–33.
37. Yancy CW, Jessup M, Bozkurt B, Butler J, Casey DE, Drazner MH, et al. 2013 ACCF/AHA guideline for the management of heart failure: A report of the american college of cardiology foundation/american heart association task force on practice guidelines. Circulation. 2013;128(16):1810–52.
38. McMurray JJV. Systolic Heart Failure. N Engl J Med. 2010;362(3):228–38.
39. Aurigemma GP, Gaasch WH. Diastolic Heart Failure. N Engl J Med. 2004;351:1097–105.
40. Pugliese NR, Fabiani I, La Carrubba S, Conte L, Antonini-Canterin F, Colonna P, et al. Classification and Prognostic Evaluation of Left Ventricular Remodeling in Patients With Asymptomatic Heart Failure. Am J Cardiol. 2017;119(1):71–7.
41. Y, Gerber, Weston S, Enriquez-Sarano M, Berardi C, Chamberlain A, Manemann S, Jiand R, Dunlay S R V. Mortality Associated With Heart Failure After Myocardial Infarction: A Contemporary Community Perspective. Circ Hear Fail. 2017;1(1):1–15.
42. Stolfo D, Cinquetti M, Merlo M, Santangelo S, Barbati G, Alonge M, et al. ST-elevation myocardial infarction with reduced left ventricular ejection fraction: Insights into persisting left ventricular dysfunction. A pPCI-registry analysis. Int J Cardiol. 2016;215:340–5.
43. Sutton MGSJ, Sharpe N. Left Ventricular Remodeling After Myocardial Infarction : Pathophysiology and Therapy. Circulation. 2000;101(25):2981–8.
44. Pfeffer MA, Braunwald E. Ventricular remodeling after myocardial infarction: Experimental observations and clinical implications. Circulation. 1990;81(4):1161–72.

45. Huttin O, Coiro S, Selton-Suty C, Juillière Y, Donal E, Magne J, et al. Prediction of left ventricular remodeling after a myocardial infarction: Role of myocardial deformation: A systematic review and meta-analysis. PLoS One. 2016;11(12):1–15.
46. Reis Filho JR de AR, Cardoso JN, Cardoso CM dos R, Pereira-Barretto AC. Reverse Cardiac Remodeling: A Marker of Better Prognosis in Heart Failure. Arq Bras Cardiol. 2015;104(6):502–6.
47. Patten RD, Soman P. Prevention and reversal of LV remodeling with neurohormonal inhibitors. Vol. 6, Curr Treat Options Cardiovasc Med. 2004. p. 313–25.
48. Kloner RA, Bolli R, Marban E, Reinlib L, Braunwald E. Medical and cellular implications of stunning, hibernation, and preconditioning: An NHLBI workshop. In: Circulation. 1998. p. 1848–67.
49. Kramer CM, Rogers WJ, Theobald TM, Power TP, Petruolo S, Reichek N. Remote noninfarcted region dysfunction soon after first anterior myocardial infarction: A magnetic resonance tagging study. Circulation. 1996;94(4):660–6.
50. Cerqueira MD, Weissman NJ, Dilsizian V, Jacobs AK, Kaul S, Laskey WK, et al. Standardized myocardial segmentation and nomenclature for tomographic imaging of the heart. J Cardiovasc Magn Reson. 2002;4(2):203–10.
51. Lanzer P, Botvinick EH, Schiller NB, Crooks LE, Arakawa M, Kaufman L, et al. Cardiac imaging using gated magnetic resonance. Radiology. 1984;150(1):121–7.
52. Ehman RL, McNamara MT, Pallack M, Hricak H, Higgins CB. Magnetic resonance imaging with respiratory gating: Techniques and advantages. Am J Roentgenol. 1984;143(6):1175–82.
53. Soneson H, Ubachs JFA, Ugander M, Arheden H, Heiberg E. An Improved Method for Automatic Segmentation of the Left Ventricle in Myocardial Perfusion SPECT. J Nucl Med. 2009;50(2):205–13.
54. Ugander M, Soneson H, Engblom H, van der Pals J, Erlinge D, Heiberg E, et al. Quantification of myocardium at risk in myocardial perfusion SPECT by co-registration and fusion with delayed contrast-enhanced magnetic resonance imaging - an experimental ex vivo study. Clin Physiol Funct Imaging. 2012;32(1):33–8.
55. Pocock SJ, Ariti C a, McMurray JJV, Maggioni A, Køber L, Squire IB, et al. Predicting survival in heart failure: A risk score based on 39 372 patients from 30 studies. Eur Heart J. 2013;34(19):1404–13.
56. Rahimi K, Bennett D, Conrad N, Williams TM, Basu J, Dwight J, et al. Risk prediction in patients with heart failure: A systematic review and analysis. JACC Hear Fail. 2014;2(5):440–6.
57. Lupon J, Vila J, Bayes-Genis A. Risk prediction tools inpatients with heartfailure. JACC Hear Fail. 2015;3(3):267.
58. Höglund C, Alam M, Thorstrand C. Atrioventricular Valve Plane Displacement in Healthy Persons: An Echocardiographic Study. Acta Med Scand. 1988;224(6):557–62.
59. Kawel-Boehm N, Maceira A, Valsangiacomo-Buechel ER, Vogel-Claussen J, Turkbey EB, Williams R, et al. Normal values for cardiovascular magnetic resonance in adults and children. J Cardiovasc Magn Reson. 2015;17(1):29.
60. Lundbäck S. Cardiac pumping and function of the ventricular septum. Vol. 550, Acta Physiologica Scandinavica. Supplementum. 1986.

61. Hu K, Liu D, Herrmann S, Niemann M, Gaudron PD, Voelker W, et al. Clinical implication of mitral annular plane systolic excursion for patients with cardiovascular disease. Vol. 14, European Heart Journal Cardiovascular Imaging. 2013. p. 205–212. Review.
62. Alam M, Höglund C, Thorstrand C. Longitudinal systolic shortening of the left ventricle: an echocardiographic study in subjects with and without preserved global function. Clin Physiol. 1992;Jul(12;(4)):443–52.
63. Ugander M, Cain P a, Perron A, Hedström E, Arheden H. Infarct transmurality and adjacent segmental function as determinants of wall thickening in revascularized chronic ischemic heart disease. Clin Physiol Funct Imaging. 2005;25(4):209–14.
64. Nowosielski M, Schocke M, Mayr A, Pedarnig K, Klug G, Köhler A, et al. Comparison of wall thickening and ejection fraction by cardiovascular magnetic resonance and echocardiography in acute myocardial infarction. J Cardiovasc Magn Reson. 2009;11:22.
65. Tustison NJ, Dávila-Román VG, Amini AA. Myocardial kinematics from tagged MRI based on a 4-D B-spline model. IEEE Trans Biomed Eng. 2003;50(8):1038–40.
66. Young A a, Imai H, Chang CN, Axel L. Two-dimensional left ventricular deformation during systole using magnetic resonance imaging with spatial modulation of magnetization. Circulation. 1994;89(2):740–52.
67. Riffel JH, Andre F, Maertens M, Rost F, Keller MGP, Giusca S, et al. Fast assessment of long axis strain with standard cardiovascular magnetic resonance: A validation study of a novel parameter with reference values. J Cardiovasc Magn Reson. 2015;17(1):1–9.
68. Moore CC, Lugo-Olivieri CH, McVeigh ER, Zerhouni EA. Three-dimensional Systolic Strain Patterns in the Normal Human Left Ventricle: Characterization with Tagged MR Imaging. Radiology. 2000;214(2):453–66.
69. Chitiboi T, Axel L. Magnetic resonance imaging of myocardial strain: A review of current approaches. J Magn Reson Imaging. 2017;46(5):1263–80.
70. Mangion K, McComb C, Auger DA, Epstein FH, Berry C. Magnetic Resonance Imaging of Myocardial Strain After Acute ST-Segment-Elevation Myocardial Infarction: A Systematic Review. Circ Cardiovasc Imaging. 2017;10(8):1–10.
71. Axel L, Dougherty L. MR imaging of motion with spatial modulation of magnetization. Radiology. 1989;171(3):841–5.
72. Amundsen BH, Helle-Valle T, Edvardsen T, Torp H, Crosby J, Lyseggen E, et al. Noninvasive myocardial strain measurement by speckle tracking echocardiography: Validation against sonomicrometry and tagged magnetic resonance imaging. J Am Coll Cardiol. 2006;47(4):789–93.
73. Van Dijk P. Direct cardiac nmr imaging of heart wall and blood flow velocity. J Comput Assist Tomogr. 1984;8(3):429–36.
74. Hor KN, Baumann R, Pedrizzetti G, Tonti G, Gottliebson WM, Taylor M, et al. Magnetic Resonance Derived Myocardial Strain Assessment Using Feature Tracking. J Vis Exp. 2011;12(48):pii:2356.
75. Kuetting D, Sprinkart AM, Doerner J, Schild H, Thomas D. Comparison of magnetic resonance feature tracking with harmonic phase imaging analysis (CSPAMM) for assessment of global and regional diastolic function. Eur J Radiol. 2015;84(1):100–7.
76. Wu L, Germans T, Güçlü A, Heymans MW, Allaart CP, Van Rossum AC. Feature tracking compared with tissue tagging measurements of segmental strain by cardiovascular magnetic resonance. J Cardiovasc Magn Reson. 2014;16(10).

77. Aletras AH, Ding S, Balaban RS, Wen H. DENSE: Displacement Encoding with Stimulated Echoes in Cardiac Functional MRI. J Magn Reson. 1999;137(1):247–52.
78. Neizel M, Lossnitzer D, Korosoglou G, Schäufele T, Lewien A, Steen H, et al. Strain-encoded (SENC) magnetic resonance imaging to evaluate regional heterogeneity of myocardial strain in healthy volunteers: Comparison with conventional tagging. J Magn Reson Imaging. 2009;29(1):99–105.
79. Erlinge D, Götberg M, Lang I, Holzer M, Noc M, Clemmensen P, et al. Rapid endovascular catheter core cooling combined with cold saline as an adjunct to percutaneous coronary intervention for the treatment of acute myocardial infarction. The CHILL-MI trial: a randomized controlled study of the use of central venous cathete. J Am Coll Cardiol. 2014;63(18):1857–65.
80. Atar D, Arheden H, Berdeaux A, Bonnet J-L, Carlsson M, Clemmensen P, et al. Effect of intravenous TRO40303 as an adjunct to primary percutaneous coronary intervention for acute ST-elevation myocardial infarction: MITOCARE study results. Eur Heart J. 2014;36(2):1–8.
81. Hedström E, Engblom H, Frogner F, Åström-olsson K, Öhlin H, Jovinge S, et al. Infarct evolution in man studied in patients with first-time coronary occlusion in comparison to different species - implications for assessment of myocardial salvage. J Cardiovasc Magn Reson. 2009;10:1–10.
82. Arheden H, Saeed M, Higgins CB, Gao D-W, Bremerich J, Wyttenbach R, et al. Measurement of the Distribution Volume of Gadopentetate Dimeglumine at Echo-planar MR Imaging to Quantify Myocardial Infarction: Comparison with ^{99m} Tc-DTPA Autoradiography in Rats. Radiology. 1999;
83. Kim RJ, Fieno DS, Parrish TB, Harris K, Chen EL, Simonetti O, et al. Relationship of MRI delayed contrast enhancement to irreversible injury, infarct age, and contractile function. Circulation. 1999;100(19):1992–2002.
84. Mahrholdt H, Wagner A, Holly TA, Elliott MD, Bonow RO, Kim RJ, et al. Reproducibility of chronic infarct size measurement by contrast-enhanced magnetic resonance imaging. Circulation. 2002;106(18):2322–7.
85. Kim RJ, Wu E, Rafael A, Chen E-L, Parker MA, Simonetti O, et al. The Use of Contrast-Enhanced Magnetic Resonance Imaging to Identify Reversible Myocardial Dysfunction. N Engl J Med. 2000;343(20):1445–53.
86. Heiberg E, Ugander M, Engblom H, Götberg M, Olivecrona GK, Erlinge D, et al. Automated quantification of myocardial infarction from MR images by accounting for partial volume effects: animal, phantom, and human study. Radiology. 2008;246(2):581–8.
87. Carlsson M, Ubachs JFA, Hedström E, Heiberg E, Jovinge S, Arheden H. Myocardium at Risk After Acute Infarction in Humans on Cardiac Magnetic Resonance. Quantitative Assessment During Follow-Up and Validation With Single-Photon Emission Computed Tomography. JACC Cardiovasc Imaging. 2009;2(5):569–76.
88. Bogaert J, Rademakers FE. Regional nonuniformity of normal adult human left ventricle. AmJPhysiol Hear CircPhysiol. 2001;280:610–20.
89. Kidambi A, Mather AN, Swoboda P, Motwani M, Fairbairn TA, Greenwood JP, et al. Relationship between Myocardial Edema and Regional Myocardial Function after Reperfused Acute Myocardial Infarction: An MR Imaging Study. Radiology. 2013;267(3):701–8.
90. Braunwald E, Kloner R a. The stunned myocardium: Prolonged, postischemic ventricular dysfunction. Vol. 66, Circulation. 1982. p. 1146–1149. Review.

91. Binek A, Fernández-Jiménez R, Jorge I, Camafeita E, López JA, Bagwan N, et al. Proteomic footprint of myocardial ischemia/reperfusion injury: Longitudinal study of the at-risk and remote regions in the pig model. Sci Rep. 2017;7(1):1–16.
92. Støylen A. Basic concepts in myocardial strain and strain rate. Available from: http:folk.ntnu.no/Støylen/strainrate/Regional_systolic#AV_plane
93. Rangarajan V, Chacko SJ, Romano S, Jue J, Jariwala N, Chung J, et al. Left ventricular long axis function assessed during cine-cardiovascular magnetic resonance is an independent predictor of adverse cardiac events. J Cardiovasc Magn Reson. 2016;18(1):35.
94. Rosendahl L, Blomstrand P, Brudin L, Tödt T, Engvall JE. Longitudinal peak strain detects a smaller risk area than visual assessment of wall motion in acute myocardial infarction. Cardiovasc Ultrasound. 2010;8(2).
95. Støylen A, Skjærpe T. Systolic long axis function of the left ventricle . Global and regional information. Scand Cardiovasc J. 2003;37(5):253–8.
96. Garg P, Broadbent DA, Swoboda PP, Foley JRJ, Fent GJ, Musa TA, et al. Extra-cellular expansion in the normal, non-infarcted myocardium is associated with worsening of regional myocardial function after acute myocardial infarction. J Cardiovasc Magn Reson. 2017;19(1).
97. Everaars H, Robbers LFHJ, Götte M, Croisille P, Hirsch A, Teunissen PFA, et al. Strain analysis is superior to wall thickening in discriminating between infarcted myocardium with and without microvascular obstruction. European Radiology. 2018;1–11.
98. Ingul CB, Malm S, Refsdal E, Hegbom K, Amundsen BH, Støylen A. Recovery of Function After Acute Myocardial Infarction Evaluated by Tissue Doppler Strain and Strain Rate. J Am Soc Echocardiogr. 2010;23(4):432–8.
99. Engblom H, Hedstrom E, Heiberg E, Wagner GS, Pahlm O, Arheden H. Rapid initial reduction of hyperenhanced myocardium after reperfused first myocardial infarction suggests recovery of the peri-infarction zone one-year follow-up by MRI. Circ Cardiovasc Imaging. 2009;2(1):47–55.
100. Hassell MECJ, Vlastra W, Robbers L, Hirsch A, Nijveldt R, Tijssen JGP, et al. Long-term left ventricular remodelling after revascularisation for ST-segment elevation myocardial infarction as assessed by cardiac magnetic resonance imaging. Open Hear. 2017;4(1):1–7.